Published December 15, 2008

Ly49Q is normally expressed at low levels on this cell type. Collectively, these data demonstrate that the open reading frame of $Ly49q_1$ was disrupted successfully.

The effect of introducing *PGK-neo* or a *loxP* site in $Ly49q_1$ on neighboring gene expression was assessed by flow cytometry on both resting and IL-2–cultured NK cells with mAb recognizing proteins encoded by genes 5′ (*Ly49g*, *Ly49r*, and *Ly49e/s*) and 3′ (*Nkg2a/c/e* and *Nkg2d*) of $Ly49q_1$. Both the distribution and lmean fluorescence intensity (MFI) of these receptors were the same on $Ly49q^{wt/wt}$, $Ly49q^{neo/neo}$, and $Ly49q^{lox/lox}$ NK cells (unpublished data). This indicates that the targeted insertion had no secondary effect on other genes located within the natural killer gene complex. Furthermore, Ly49Q-null pDC H-2K^b and H-2D^b surface levels were identical to those of Ly49Q-WT pDCs (unpublished data). As $Ly49q_2$ and q_3 are likely pseudogenes, $Ly49q_1$ will be referred to as *Ly49q* hereafter. Unless otherwise stated, all experiments were performed with $Ly49q^{wt/wt}$ (WT) or $Ly49q^{lox/lox}$ (Ly49Q-null) littermates in the high IFN-producing 129 background.

Hematopoiesis and pDC development in Ly49Q-null mice

Fresh splenic pDCs are round cells with eccentric kidney-shaped nuclei, as visualized by Giemsa stain (Fig. 3 A). After activation with CpG-ODN, pDCs were larger and displayed a higher cytoplasmic to nucleus content, and the cytoplasm also appeared more vacuolated. The size and morphology of resting or activated pDCs from Ly49Q-WT and -null mice were similar. To determine whether the localization of Ly49Q-null

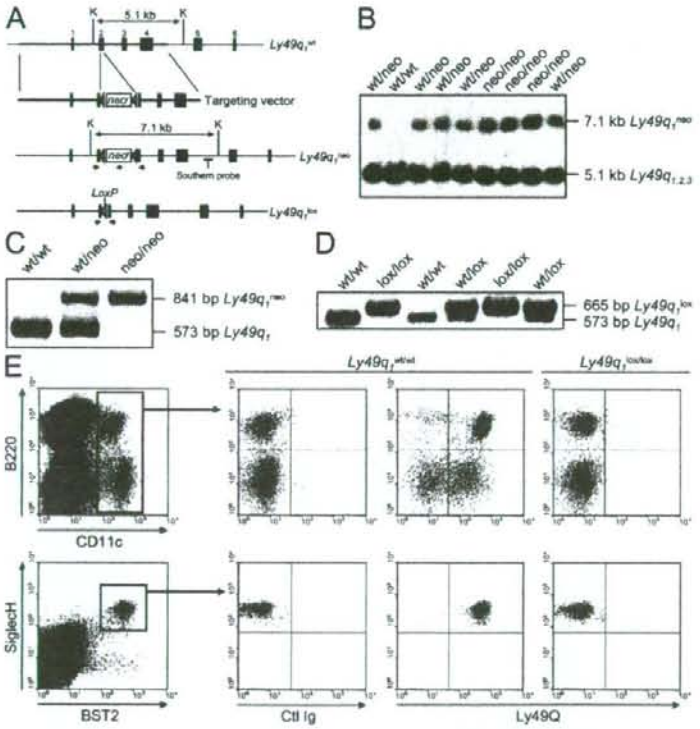

Figure 2. Generation of Ly49Q-null mice. (A) $Ly49q_1$ gene disruption strategy. A 10-kb segment encompassing exons 1–4 was cloned by recombineering from BAC DNA, and a floxed *PGK-Neo*^{r} (*neo*^{r}) cassette was inserted into exon 2. After electroporation and selection, an ES clone possessing the predicted KpnI (K) fragment, as verified by Southern blotting, was electroporated with CMV-Cre plasmid, and the deletion of *PGK-Neo*^{r} was confirmed by PCR. Both $Ly49q_1^{neo}$ and $Ly49q_1^{lox}$ mice were created. PCR primers are shown by arrowheads. Boxes denote exons, and the location of the Southern probe is underlined. (B) Southern blot analysis. Genomic tail DNA of pups from $Ly49q_1^{neo/wt}$ parent mice was digested with KpnI and analyzed by Southern blotting with the probe depicted in A. Note that the probe detects identical fragments from $Ly49q_1$, q_2, and q_3 genes. (C) PCR analysis of tail DNA from mice in B. To eliminate confusion caused by $Ly49q_2$ and q_3 genes, $Ly49q_1$-specific primers were designed. These primers were used to analyze tail DNA by PCR and to differentiate between $Ly49q_1^{wt}$ and $Ly49q_1^{neo}$ alleles. (D) PCR analysis of pups from $Ly49q_1^{lox/wt}$ parent mice. Tail DNA was PCR amplified with primers flanking exon 2 to differentiate $Ly49q_1^{wt}$ and $Ly49q_1^{lox}$ alleles. (E) Lack of Ly49Q protein on DCs derived from Ly49Q-null mice. Ly49Q-null and -WT splenocytes were stained with a combination of mAb to CD11c/B220 (top) or Siglec-H/BST2 (bottom), and Ly49Q-specific mAb NS-34 or an isotype control. Ly49Q mAb staining intensity relative to isotype control mAb on gated cells is shown.

Published December 15, 2008

pDCs is normal, three-color immunofluorescent staining using mPDCA-1, CD3, and CD19 mAbs was performed on splenic sections from untreated and CpG-ODN–treated animals. In the spleens of untreated animals, pDCs were mainly localized within the T cell zones and in lower numbers within marginal zone and red pulp (Fig. 3 B). In CpG-ODN–treated animals, the number of pDCs was increased and they tended to form clusters (Fig. 3 B). The majority of CpG-activated pDCs were found within the marginal zone and red pulp, as previously reported (23). Thus, no significant differences were observed in the localization of pDCs in WT and Ly49Q-null mice before or after CpG-ODN treatment.

The potential effect of Ly49Q absence on pDC frequency and distribution of cells in primary and secondary lymphoid organs was investigated in the Ly49Q-null mice. The pDC population as defined by CD11c$^+$Siglec-H$^+$ showed no significant difference in the proportion and total number of pDCs in the spleen, mesenteric lymph nodes, or bone marrow of young mice (6 wk old; Fig. 3 C and not depicted). However, in older mice (>9 mo old) there was approximately a twofold increase in the proportion and total number of pDCs in these organs (Fig. 3 C and not depicted). Myeloid lineage cells in various organs have been reported to express Ly49Q. There were no significant differences in the percentage and total number of CD11b$^+$Gr-1$^+$ cells in the bone marrow, spleen, or lymph nodes in either young or old mice (unpublished data). Similarly, blood neutrophil numbers and proportion in WT mice and Ly49Q-null littermates were not significantly different (unpublished data). In fact, no significant difference for any lineage tested was observed, including the B, NK, NKT, CD4$^+$ T, or CD8$^+$ T cells, or mDC subsets in either young or old mice (unpublished data). Therefore, Ly49Q deficiency appears to selectively affect pDC development and homeostasis, albeit only modestly. Young mice (5–8 wk old) were chosen for all functional experiments.

Severe defect in TLR9-induced IFN-α production by Ly49Q-null pDCs

To determine the effect of Ly49Q deficiency on pDC activation and subsequent cytokine production, the response of Ly49Q-null pDCs to TLR9 agonists was evaluated. Splenic pDCs were isolated from WT and Ly49Q-null littermates using mPDCA-1–conjugated magnetic beads, cultured overnight in various concentrations of CpG-ODN, and the supernatant was assayed for IFN-α. Remarkably, Ly49Q-null pDC supernatants yielded approximately fivefold lower levels of IFN-α relative to supernatants from identically treated WT pDCs (Fig. 4 A). This finding is consistent with the earlier observation that Ly49Q binding to H-2K^b is necessary for TLR9-mediated IFN-α secretion (Fig. 1 A). In parallel, Ly49Q-deficient pDCs showed a significant defect in IL-12 secretion in response to CpG-ODN compared with WT pDCs (Fig. 4 B). The IL-12 defect was not as pronounced as that observed for IFN-α but is consistent with the decrease in IL-12 production observed upon mAb-mediated blockade of Ly49Q–H-2K^b interactions (Fig. 1 B). In contrast, TNF-α and IL-6

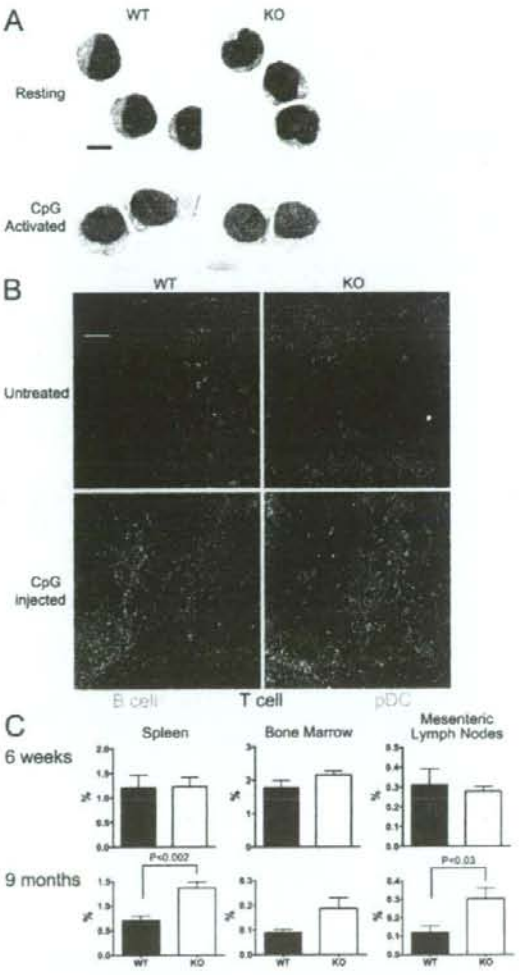

Figure 3. Age-dependent increase in pDC proportion in Ly49Q-null mice. (A) pDC size and morphology. pDCs were sorted as CD11c$^+$B220$^+$CD11b$^-$DX5$^-$CD3$^-$CD19$^-$ cells from the spleen and cytocentrifuged on microspcope slides directly as resting pDCs or after incubation with 3 μg/ml CpG for 16 h. Slides were then stained with Giemsa solution. Bar, 5 μm. (B) Localization of splenic pDCs. Sections of spleen isolated from untreated young mice or mice injected i.v. with 10 μg/ml CpG 24 h earlier were stained with fluorescently labeled mAb to CD19 (B cells; green), CD3 (T cells; blue), and BST2 (pDCs; red). Bar, 50 μm. (C) Frequency of pDCs defined as CD11c$^+$Siglec-H$^+$ cells in lymphoid organs of *Ly49q*$^{+/+}$ (closed bars) and *Ly49q*$^{lox/lox}$ (open bars) mice (6 wk old, $n = 3$; 9 mo old, $n = 6$). A similar pattern was observed with BST2 staining (not depicted). Data are presented as the mean of individual mice (error bars = SD). Results are representative of at least three independent experiments, except for C (9-mo-old mice), which was done twice.

production were not compomised in Ly49Q-deficient pDCs (Fig. 4, C and D). Thus, Ly49Q-deficient pDCs possess an intrinsic defect in IFN-α production after stimulation with TLR9 agonists in vitro.

Injection of mice with CpG-ODN leads to a rapid elevation of serum IFN-α peaking at 6 h after treatment that is mediated by pDCs (23). To determine whether the in vitro cytokine defect of Ly49Q-null pDCs had in vivo consequences, mice were injected with CpG-ODN, and serum IFN-α levels were evaluated after 6 h. Importantly, IFN-α serum levels in CpG-injected Ly49Q-null mice were consistently 5–10-fold less than those of WT littermates (Fig. 4 E). On the other hand, the sera of both cohorts showed similar levels of IL-12 (unpublished data). The normal serum IL-12 levels detected in Ly49Q-null mice after CpG injection were most likely caused by TLR9-mediated IL-12 production by cell types other than pDCs (24). A time-course experiment monitoring serum IFN-α levels confirmed that although maximal IFN-α levels occur 4–6 h after injection in WT mice, Ly49Q-null mice failed to attain a similar magnitude of IFN-α levels at any time point assayed (Fig. 4 F). Thus, Ly49Q-null mice display an inherent defect in IFN-α

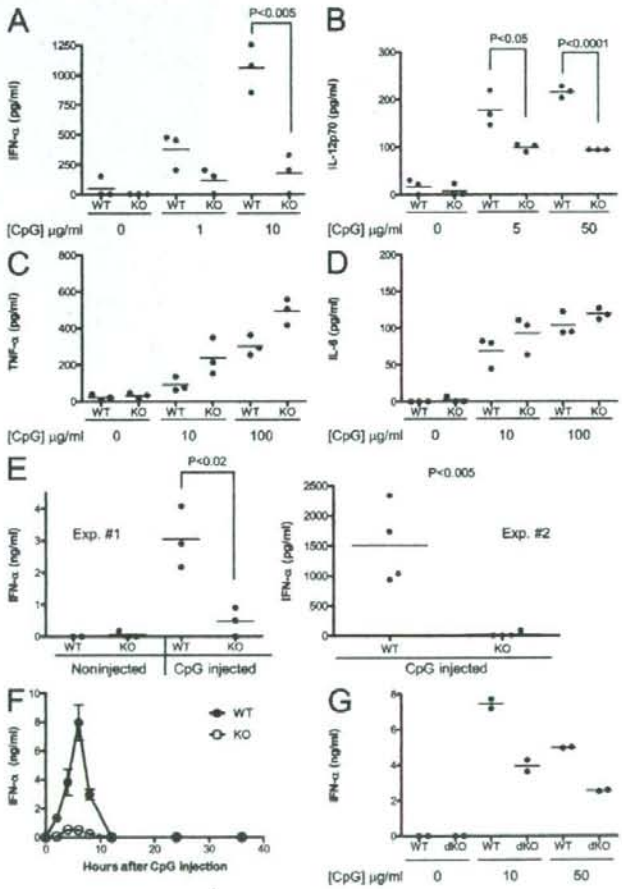

Figure 4. Ly49Q-null pDCs display an IFN-α production defect in response to CpG-ODN. (A–D) IFN-α production by isolated pDCs after CpG-ODN stimulation. pDCs were isolated with mPDCA-1 microbeads from Ly49Q-null and -WT mice and cultured overnight in the presence of the indicated concentrations of CpG-ODN. Culture supernatants were assayed by ELISA for IFN-α (A), IL-12p70 (B), TNF-α (C), or IL-6 (D). (E) Induction of serum cytokines by CpG-ODN injection. Ly49Q-null and -WT littermates were injected with CpG-ODN + DOTAP, and blood samples were taken after 6 h for IFN-α ELISA. Uninjected mice served as controls. Each symbol represents a single mouse. (F) Serum IFN-α time course after CpG-ODN stimulation. Ly49Q-null and -WT littermates were injected with CpG-ODN + DOTAP, and blood was collected periodically over 36 h. Serum IFN-α levels were deduced by ELISA from three mice of each genotype for each time point. Data are representative of experiments done at least three times independently (error bars = SD). (G) pDCs were isolated from H-2K^{b}D^b-null or -WT (B6) mice and treated as in A. Horizontal bars represent means.

Published December 15, 2008

production in vivo, and IFN-α and IL-12 responses to CpG-ODN can be uncoupled in these mice. Although the absence of the receptor leads to clear defects in cytokine production, the effect of loss of the ligand is unknown. Thus, pDCs were isolated from H-2K^{b}D^b–null mice and were stimulated for IFN-α production by CpG-ODN. H-2K^{b}D^b–null pDCs showed ~50% reduction in IFN-α secretion compared with WT pDCs (Fig. 4 G). These results are consistent with the hypothesis that Ly49Q–MHC interactions are necessary for cytokine production in pDCs, whereas the inhibition of IFN-α secretion was not as pronounced as for Ly49Q-null pDCs. Possible reasons for this difference may include the mouse strain background or that Ly49Q may have other ligands in addition to H-2K^b.

To address the question of whether Ly49Q/MHC interact in cis or trans to regulate pDC function, Ly49Q-null mice were crossed to H-2K^{b}D^b–null mice, and the resulting F1 mice were intercrossed to generate the four possible null phenotypes. pDCs from WT mice stain positively with soluble H-2K^b/OVA tetramer, and this binding is caused by Ly49Q, as shown by the complete absence of binding in Ly49Q-null mice and by previous blocking experiments with anti-Ly49Q mAb (Fig. 5 A, compare the top two dotplots) (21). In the absence of H-2K^b expression, binding of the H-2K^b tetramer is much stronger but still Ly49Q dependent (Fig. 5 A, compare the bottom two dotplots). Differential tetramer binding was not caused by differences in Ly49Q expression between WT and H-2K^{b}D^b–null mice, as pDCs from both mouse strains expressed similar levels of Ly49Q (Fig. 5 B). These results suggest that in WT pDCs, cis interactions between Ly49Q and endogenous H-2K^b are inhibiting binding of soluble H-2K^b tetramer to Ly49Q.

Normal TLR9 expression and pDC activation in Ly49Q-deficient mice

Although the in vitro mAb-mediated blocking experiments are consistent with the phenotype of Ly49Q-null pDCs in vitro and in vivo, the defect in TLR9-induced cytokine production might be the result of factors other than the absence of Ly49Q. First, Ly49Q deficiency may have caused down-regulation of TLR9. To exclude this possibility, TLR9 expression was determined by RT-PCR and intracellular flow cytometry given the localization of TLR9 in endosomes. TLR9 levels were measured and found to be similar in both Ly49Q-WT and -null pDCs (Fig. 6 A and not depicted), suggesting that Ly49Q-null pDCs have an equal potential to bind CpG-ODN. Second, the almost complete lack of IFN-α secretion by Ly49Q-null pDCs may be caused by an inability of the cells to become fully activated. Downstream activation events in pDCs both in vivo (Fig. 6 B) and in vitro (Fig. 6 C) after CpG-ODN challenge were assessed by flow cytometry analysis of CD86 and class II MHC surface expression, and were found to be normal. The percentage of pDCs expressing CD86 and the level of CD86 on pDCs were similar between WT and Ly49Q-null pDCs after CpG treatment, even over an extended range of doses (Fig. 6, B and C). Similar observations were made for class II MHC (unpublished data). Collectively, these data suggest that the signaling pathways downstream of TLR9 that induce expression of CD86/class II MHC are different from those that lead to IFN-α production such that Ly49Q signaling modulates only the latter responses in pDCs.

TLR7-mediated cytokine secretion is defective in Ly49Q-null mice

To further characterize the extent of the defect in Ly49Q-null pDC cytokine responses, a distinct TLR pathway was evaluated. In addition to high levels of TLR9, pDCs also express TLR7, which can recognize single-stranded RNA motifs represented by such viruses as influenza and vesicular stomatitis virus. Similar to CpG-ODN stimulation, infection of isolated pDCs with influenza virus resulted in high levels of secreted IFN-α, as previously reported (6). Ly49Q-null pDCs produced fivefold less IFN-α and threefold less IL-12 than WT pDCs in response to influenza (Fig. 7, A and B).

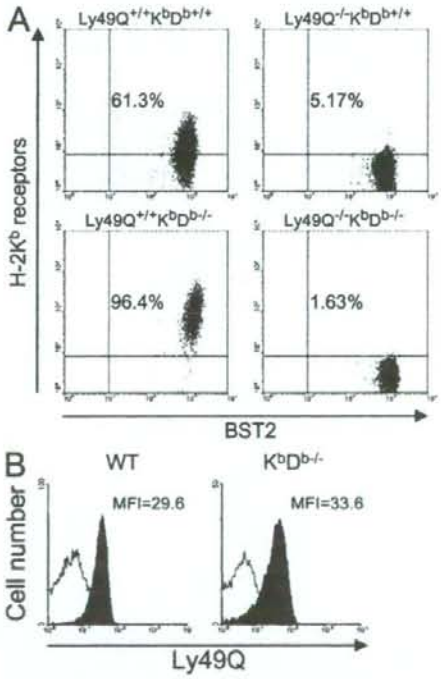

Figure 5. Ly49Q binds to H-2K^b in cis. (A) pDCs were isolated from the spleens of mice with the indicated genotypes with mPDCA-1 microbeads. Isolated pDCs were stained with PE–H-2K^b/OVA tetramer and allophycocyanin–anti-BST2 mAb and were analyzed by flow cytometry. Cells are gated on pDCs. The percentage of cells positively staining with PE–H-2K^b/OVA is shown. (B) Ly49Q levels on MHC-deficient pDCs. Splenocytes from the indicated strains (WT is B6) were stained for BST2, Siglec-H, and Ly49Q (NS34). The level of Ly49Q expression on BST2$^+$Siglec-H$^+$ cells is shown (shaded histogram). The open histogram represents the secondary reagent alone.

Active and inactivated influenza virus treatments gave similar results (unpublished data). In contrast, CD86 and class II MHC up-regulation of isolated pDCs in response to a TLR7 agonist was normal in Ly49Q-null pDCs (Fig. 7 C and not depicted). Therefore, TLR7-induced cytokine secretion is also attenuated in Ly49Q-null pDCs.

Ly49Q-deficient mice exhibit diminished protection to mouse CMV (MCMV) infection

The defect in IFN-α production seen in Ly49Q-null mice after TLR9 stimulation may have deleterious consequences during immune responses against pathogens that are detected through TLR9. Previous studies have reported that TLR9 deficiency promotes increased susceptibility to MCMV infection, as manifested by higher viral loads and defective production of multiple cytokines, including type I IFN (24, 25). As such, the defect in TLR9-dependent IFN-α production observed in Ly49Q-null mice may also lead to diminished pDC responses and altered innate immunity to DNA viruses like MCMV. In keeping with this, purified Ly49Q-null pDCs produce approximately threefold less IFN-α than WT pDCs in response to overnight MCMV infection in vitro (Fig. 8 A). The MCMV/pDC co-culture experiment confirms, independently of CpG-ODN, that pDCs from Ly49Q-null mice display defective IFN-α production when triggered through TLR9.

To confirm these findings in vivo, Ly49Q-null mice were infected with MCMV. As shown in Fig. 8 B, splenic viral titers were consistently higher in Ly49Q-null mice versus WT control animals. Although not all experiments showed a statistically significant difference between the two cohorts (e.g., day 3, 6,000 PFU; Fig. 8 B), the detection of impaired viral immunity may be complicated by the susceptible Ly49H$^-$ 129 background of these mice (26). Because

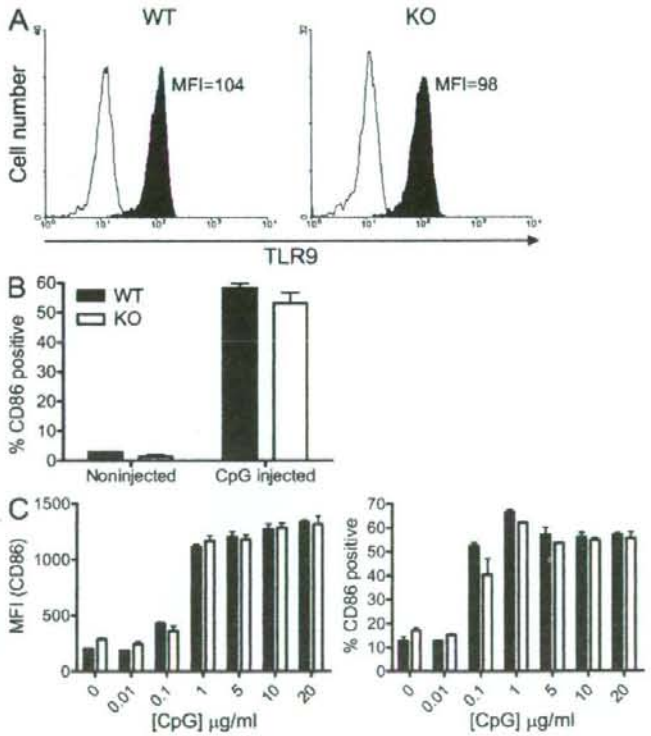

Figure 6. Normal TLR9 and CD86 expression by Ly49Q-null pDCs. (A) Splenocytes from Ly49Q-null and -WT mice were stained for Siglec-H and BST2, and were then permeabilized and stained for intracellular TLR9 or with an isotype control mAb. TLR9 (shaded histogram) or control (open histogram) expression on Siglec-H$^+$BST2$^+$ cells is shown. (B) In vivo activation of pDCs by CpG-ODN. Ly49Q-null and -WT littermates were injected with CpG-ODN + DOTAP. Uninjected mice served as controls. After 6 h, the splenocytes were isolated and stained for Siglec-H, BST2, and CD86, and were analyzed by flow cytometry. The percentage of CD86$^+$ pDCs after 6 h is shown (error bars = SD). (C) In vitro activation of pDCs by CpG-ODN. pDCs from Ly49Q-null and -WT mice were isolated with mPDCA-1 microbeads and cultured overnight in the presence of the indicated concentrations of CpG-ODN. The following day, the CD11c$^+$B220$^+$ cells were analyzed by flow cytometry for CD86 surface expression. MFI (left) and the percentage of positive cells (right) are shown as the means of triplicate cultures ± SD. Data are representative of at least three independent experiments.

Published December 15, 2008

the *Ly49h* gene conferring resistance to MCMV in B6 mice (27, 28) is <300 kb away from the targeted $Ly49q^{lacz}$ allele, these experiments could not be repeated on the MCMV-resistant B6 background at this time. Notwithstanding this, the majority of experiments did reveal a statistically significant increase in Ly49Q-null MCMV titers when performed using either an early time point (1.5 d after infection) or a low initial MCMV inoculum (600 PFU), or both (Fig. 8 B). In agreement with our findings, TLR9-null mice on a susceptible background (Ly49H$^-$ BALB/c) display a similarly small but significant increase in splenic viral titers after MCMV infection (24). Serum IFN-α and IL-12 levels peak at 36 h after MCMV infection. At this time point, Ly49Q-null mice display normal levels of IFN-α (Fig. 8 C) and slightly decreased IL-12p70 levels (Fig. 8 D). This suggests that in addition to pDCs, other cell types can contribute to serum IFN-α/IL-12 levels by 36 h after infection. Collectively, these experiments demonstrate that Ly49Q-null pDCs exhibit a functional deficiency in IFN-α production in response to MCMV infection in vitro, and this translates into an enhanced susceptibility of Ly49Q-null mice to MCMV infection in vivo.

DISCUSSION

Ly49q is a highly conserved *Ly49* found in all mouse strains characterized to date (16). Ly49Q is also unique in being expressed on pDCs, in contrast to all other Ly49s. We have previously shown, using the BWZ lacZ-based reporter cell assay, that H-2K^b is a high affinity ligand for Ly49Q (21). In this study, we confirm the specificity of Ly49Q for H-2K^b in a functional assay (IFN-α secretion) using fresh ex-vivo pDCs. Remarkably, Ly49Q–H-2K^b interactions appear to be required for optimal TLR7- and TLR9-dependent stimulation of cytokine production by pDCs, as indicated by the drastic reduction in CpG-mediated IFN-α and IL-12 secretion upon mAb-mediated blockade of either Ly49Q receptor or its cognate ligand, H-2K^b. In further support of this

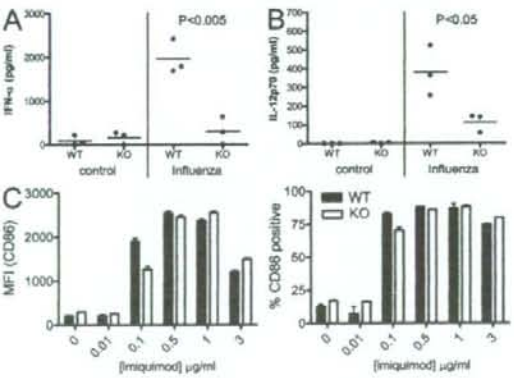

Figure 7. TLR7-induced cytokine production is defective in Ly49Q-null pDCs. (A and B) In vitro activation of pDCs by influenza virus. pDCs from Ly49Q-null and -WT mice were isolated using mPDCA-1 microbeads and cultured overnight in the presence or absence of 20 hemagglutinin units of influenza virus. Culture supernatants were assayed by ELISA for IFN-α (A) or IL-12p70 (B). Each symbol represents a single mouse. Horizontal bars represent means. (C) In vitro activation of pDCs by imiquimod. pDCs from Ly49Q-null and -WT mice were isolated using mPDCA-1 microbeads and cultured overnight with the indicated concentrations of imiquimod. The following day, CD11c$^+$B220$^+$ cells were stained with FITC–anti-CD86 and analyzed by flow cytometry for CD86 surface expression. MFI (left) and the percentage of positive cells (right) are shown as the means of triplicate cultures ± SD. Data are representative of at least three independent experiments.

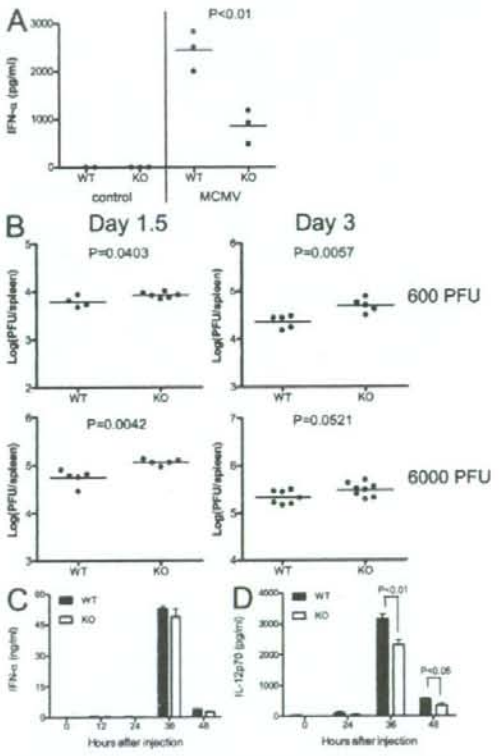

Figure 8. Reduced anti-MCMV responses by Ly49Q-null mice. (A) Decreased MCMV-induced IFN-α secretion by pDCs in vitro. Splenic pDCs were isolated with mPDCA-1 microbeads and cultured overnight in the presence of 200 PFU/ml of MCMV. Supernatants were harvested the following day. Supernatants were assayed for IFN-α levels by ELISA. (B) Greater MCMV proliferation in Ly49Q-null mice. Ly49Q-null and -WT mice were challenged with 600 or 6,000 PFU MCMV. After 1.5 or 3 d, spleens were harvested and viral titer was determined using BALB/c mouse embryo fibroblasts. Each symbol represents a single mouse. Data are representative of at least three independent experiments. Horizontal bars represent means. (C and D) Littermates of the indicated genotypes were infected with 6,000 PFU MCMV i.p., and serum samples were taken at the indicated time points after infection. IFN-α (C) or IL-12p70 (D) levels were determined by ELISA ($n = 4$ per time point). The means of individual mice ± SD are shown.

hypothesis, purified pDCs cultured in the presence of low concentrations of CpG-ODN produced high levels of IFN-α when stimulated on immobilized Ly49Q mAb or H-2K^b/Ig fusion protein but not in the presence of CpG-ODN alone. Collectively, these findings demonstrate that Ly49Q–class I MHC interactions positively regulate TLR signals and subsequent cytokine production in pDCs.

In confirmation of the in vitro mAb blocking experiments, Ly49Q-null mice show a severe defect in systemic IFN-α levels (75–100% reduction) upon challenge with CpG-ODN. This defect is likely caused by the hyporesponsiveness of Ly49Q-null pDCs, as purified pDCs from these mice exhibit similarly decreased IFN-α responses upon CpG-mediated stimulation in isolation. Ly49Q-null pDCs also show a defect in the production of IFN-α after overnight culture with MCMV. Both CpG-ODN and MCMV stimulate IFN-α production by pDCs in a TLR9-dependent manner (24). However, TLR9 mRNA and protein expression levels in Ly49Q-null pDCs are normal, as deduced by semiquantitative RT-PCR and intracellular staining, respectively. The Ly49Q-null defect similarly affects TLR7, as TLR7-dependent stimulation of isolated Ly49Q-null pDCs results in highly decreased levels of IFN-α relative to WT pDCs. Notably, in addition to IFN-α levels, Ly49Q-null pDCs also exhibit decreased IL-12p70 levels in response to CpG-ODN or influenza stimulation. Thus, Ly49Q-null pDCs possess an intrinsic cytokine production defect in response to TLR7 and TLR9 agonists. Interestingly, however, the activation status of Ly49Q-null pDCs seems normal over a wide range of CpG-ODN concentrations, at least with respect to up-regulation of CD86 and class II MHC surface expression, TNF-α and IL-6 production, morphological change, and migration within the spleen. This suggests that TLR9 stimulation results in multiple signaling pathways leading to pDC activation, but that Ly49Q regulates only the signal transduction pathway leading to IFN-α secretion.

The phenotype of pDCs from Ly49Q-null mice is similar to that observed for Ly49Q-negative pDCs from WT bone marrow. Omatsu et al. found that Ly49Q-negative pDCs produced significantly less IFN-α/β than their Ly49Q-positive counterparts when cultured in the presence of CpG-ODN or Sendai virus (19). In contrast, Kamogawa-Schifter et al. observed comparable IFN-α production levels from the two pDC subsets in vitro after stimulation with CpG-ODN (11). It is not immediately clear why there is a discrepancy in IFN-α production among Ly49Q-positive versus -negative pDCs in these two studies, as similar isolation procedures and the same mouse strain (BALB/c) were used. The data presented in this paper agree with the former study, in that the ability of pDCs to produce large amounts of IFN-α appears to depend on Ly49Q expression and function.

The positive regulation of TLR9 signaling by Ly49Q is at first counterintuitive, given that the ITIM-bearing Ly49Q receptor has the characteristics of an inhibitory Ly49 family member. Similar Ly49 receptors expressed by NK cells undergo tyrosine phosphorylation of their cytoplasmic ITIM in response to receptor engagement, resulting in the recruitment of SHP-1/2 (29). Ly49-associated SHP-1/2 are then thought to antagonize stimulatory signals initiated through ITAM-bearing adaptor molecules such as DAP12. For example, the ITIM-bearing Ly49G receptor has been demonstrated to suppress DAP12-dependent Ly49D-mediated cytotoxicity and cytokine production (30). Notably, the ability of the Ly49Q ITIM to associate with SHP-1/2 is intact, at least in reconstitution experiments using transfected cell lines (10). Thus, if Ly49Q is an inhibitory receptor, how does it function to relay TLR7/9-induced signals or amplify TLR7/9-mediated signal transduction? Interestingly, there are clues from experiments performed using DAP12-null mice that may offer a possible mechanism. Specifically, DAP12-null pDCs were reported to produce significantly more IFN-α after CpG-ODN stimulation (31), as opposed to the decreased response of Ly49Q-null mice. The resulting conclusion was that DAP12 may negatively regulate TLR7/9 signal transduction and, in turn, that DAP12-coupled receptors on pDCs may inhibit IFN-α secretion upon cross-linking. In support of this hypothesis, the pDC-expressed and DAP12-associated surface proteins Nkp44 and Siglec-H do indeed inhibit CpG-induced IFN-α secretion upon mAb-mediated ligation (12, 22). In this respect, macrophages and pDCs are functionally similar, as macrophages from DAP12-null mice produce more cytokines after TLR engagement (32). Furthermore, the DAP12-coupled TREM2 surface receptor appears to deliver constitutive inhibitory signals in macrophages (33).

The apparent stimulatory role of Ly49Q in pDCs could be caused by antagonism of inhibitory DAP12 signal transduction by SHP-1/2 recruited as a result of Ly49Q–MHC interaction. In this model, DAP12 signaling would be constitutive like TREM2 function in macrophages (33). Although the convergence point between the DAP12 and TLR9 signaling pathways is unclear, another possibility is that downstream Ly49Q signaling molecules may directly regulate the TLR9 signaling cascade independently of DAP12 function. A third mechanism behind Ly49Q function may include an alternative signaling pathway found in pDCs, one which is distinct from canonical inhibitory Ly49 signaling in NK cells and does not involve the recruitment of tyrosine phosphatases. Evidence for this possibility includes Ly49Q-transfected macrophage cell lines, which show an increase in tyrosine-phosphorylated proteins in whole-cell lysates after mAb-mediated cross-linking of Ly49Q (10).

The mechanistic link between Ly49Q function and IFN-α secretion is unknown. However, an interesting parallel may exist between NK cells and pDCs in this regard. Two reports have suggested that mature splenic NK cells lacking all self-specific MHC-binding inhibitory receptors (NKG2A and Ly49C/I in B6 mice) are hyporesponsive with respect to the killing of target cells and the production of IFN-γ (34, 35). Thus, B6 strain NK cells expressing NKG2A and/or Ly49C/I have been referred to as being "licensed" or "armed." It is tempting to speculate that pDCs like NK cells may also require the expression of at least one self-specific MHC-binding

Published December 15, 2008

inhibitory receptor to become fully functional IFN-α producers. This hypothesis is consistent with the hyporesponsiveness observed for immature Ly49Q-negative pDCs (19). Because Ly49Q binds with high affinity to H-2K^b, a self-specific determinant expressed in 129 strain Ly49Q-null mice, the lack of a self-MHC–specific inhibitory signal during pDC development in Ly49Q-null mice may render these cells anergic. However, the recapitulated phenotype using WT pDCs in mAb blocking experiments (Fig. 1) argues against Ly49Q-null pDCs being anergic.

Type I IFN is indispensable for resistance to a wide range of viruses, as shown by studies using IFN-α/βR-null mice (36). Ly49Q-null mice, which are on the Ly49H$^-$ 129 background, also display a severe IFN production defect, as well as a consistent and statistically significant increase in susceptibility to MCMV. However, the susceptibility of Ly49Q-null mice to virus infection is not as profound as that observed in IFN-α/βR-null mice. There are several possible reasons for this observation. First, although the magnitude of the IFN-α response to CpG-ODN challenge in WT mice far exceeds that of Ly49Q-null mice, the latter still yield up to 15–25% of WT serum IFN-α levels. This lower yet detectable IFN-α production may be sufficient to mount resistance to viral infection. This hypothesis is consistent with the phenotype of Ly49H$^+$ B6 mice, which produce low levels of IFN-α (6) but are nonetheless sufficient for protection against MCMV and other viruses. In agreement with our study, TLR9-null mice on a BALB/c (MCMV susceptible; Ly49H$^-$) background also only show a small increase in susceptibility (24), as would be expected if Ly49Q does indeed regulate TLR signaling. Furthermore, normal systemic IFN-α levels were observed in Ly49Q-null mice 36 h after MCMV infection despite their defective IFN-α responses to synthetic CpG-ODN. Therefore, although pDC cytokine production is compromised in Ly49Q-deficient mice and does confer limited susceptibility to viral infection, the residual capacity of these mice to produce antiviral cytokines probably affords sufficient protection. Whether these residual cytokines are made by Ly49Q-null pDCs or other cell types is not clear.

Based on the data generated from mAb-mediated blocking assays and functional analyses of Ly49Q-null pDCs in vitro, as well as in vivo analyses of Ly49Q-null mice, we conclude that pDC function, in particular IFN-α secretion, is regulated by class I MHC. The ability of pDCs to recognize class I MHC molecules is imparted by the lectin-like Ly49Q receptor, which in turn potentiates the capacity of pDCs to produce cytokines in response to TLR7 and TLR9 agonists. Loss of this self-recognition mechanism results in severe defects in IFN-α and IL-12 production by pDCs. Thus, Ly49Q–MHC interactions positively regulate pDC cytokine production triggered through TLR. Therefore, the down-regulation of class I MHC by certain viruses like MCMV could also result in the attenuation of pDC antiviral defense mechanisms in addition to evasion of CD8$^+$ T cell responses. Interestingly, despite bearing a consensus ITIM sequence, the function of Ly49Q on pDCs appears to be stimulatory in nature. Although this is somewhat paradoxical, it is nonetheless consistent with the reported counterregulatory function of DAP12-coupled receptors in pDCs, which appear to be inhibitory.

MATERIALS AND METHODS

Mice. 129S1 and B6 mice were purchased from the Jackson Laboratory. *H-2Kb^{tm1}H-2Db^{tm1}* (K^{b}D^b-KO) mice on a B6 background were purchased from Taconic. Mice were maintained and bred in the Clinical Research Institute of Montréal (IRCM) specific pathogen-free animal facilities. All manipulations performed on animals were in accordance with IRCM guidelines and were approved by the IRCM Animal Ethics Committee. Unless otherwise mentioned, all mice used for experiments were 5–8 wk of age.

Generation of Ly49Q-null mice. We previously identified 129S6 bacterial artificial chromosome (BAC) clones containing *Ly49q$_1$* (15). A 10-kb segment centered on exon 2 was retrieved from BAC 34o6 into the pMCIT-KpANhe vector by lambda red–mediated recombineering in EL350 cells, as previously described (37). To complete the targeting construct, a floxed PGK-neomycin cassette from PL400 was inserted into a unique StuI site in exon 2. The complete targeting construct sequence was confirmed. R1 ES cells (129Sv × 129Sv-CP) were electroporated with NotI-linearized targeting vector DNA and were then selected in G418. Homologous recombination in ES cells was assessed by Southern blotting. A homologous recombination efficiency of 1% was observed (6 out of 600). The germline competency of these clones was confirmed by generating heterozygous founder mice, which were then bred to achieve Ly49Q$^{neo/neo}$ homozygosity. An ES clone carrying a properly targeted *Ly49q$_1^{neo}$* allele was electroporated with a CMV-Cre vector (a gift from D. Lohnes, University of Ottawa, Ottawa, Canada) and screened for neomycin deletion by PCR. *Ly49q$_1^{neo}$* and *Ly49q$_1^{lox}$* founder mice were generated by the IRCM MicroInjection Service. Founder mice that could transmit the targeted *Ly49q$_1$* allele to the germline were bred to 129S1 females to maintain a 129 background, which was confirmed for the *Ly49* locus by 4E5 versus 12A8 staining of NK cells, as previously described (38). The resulting heterozygous mice were bred, and homozygous WT and Ly49Q-null littermates were used in all experiments unless otherwise indicated. Southern blot analysis for the *Ly49q^{neo}* allele was performed using an intron 4 probe cloned into pCR2.1TOPO (Invitrogen), prepared by amplifying BAC 34o6 DNA with 5′-TATGACTTCTTGGAGAGAGT-3′ (sense primer) and 5′-TTCACGTGGGCCTAGAATTT-3′ (antisense primer). The *Ly49q$_1^{lox}$* allele was detected by PCR with 5′-CCTAAAAGTAATTGCTGTGACTATT-3′ (sense primer) and 5′-CTTTCTAACTAGCTAACAACAG-3′ (antisense primer). A substitute reverse primer, 5′-CCGAATATCATGGTGGAAAATGGC-3′, was used to amplify the *Ly49q$_1^{neo}$* allele. The following PCR cycling parameters used were: 94°C for 30 s, 55.5°C for 30 s, and 72°C for 30 s, for 35 cycles.

pDC isolation and in vitro activation. Mouse spleens were injected with collagenase (Roche), minced, and incubated for 20 min at 37°C. After incubation, splenocytes were crushed in cold PBS-BSA-EDTA and strained through a 70-μM filter. RBCs were removed by incubation with ACK lysis buffer for 5 min at 4°C. Isolated splenocytes were maintained throughout the procedure in cold PBS-BSA-EDTA. Anti-mPDCA-1–conjugated microbead (Miltenyi Biotec) labeling was performed according to the manufacturer's protocol. Isolated pDCs were seeded at 100,000 cells per well in 200 μl of pDC medium (RPMI 1640, 10% FBS, pen/strep, L-glutamine, 2-β-mercaptoethanol) and cultured for 16 h at 37°C in 5% CO_2 in a humidified atmosphere in the presence of CpG-ODN 10103 or 2336 (Coley Pharmaceuticals), imiquimod, MCMV, or influenza at the indicated concentrations/PFU/hemagglutinin units. Supernatants were collected and frozen.

In vivo pDC activation. Mice were injected through the tail vein with CpG-ODN plus 1,2-dioleoyloxy-3-trimethylammonium-propane

Published December 15, 2008

(DOTAP; Roche) preparation (170 µl CpG-ODN diluted in sterile PBS plus 30 µl DOTAP) or imiquimod (R-837; InvivoGen) in 200 µl PBS. Mice were bled through the cheek vein at the indicated time points after injection. Serum was analyzed by ELISA.

Virus infections. Influenza strain A HK X31 H3N2 was a gift from T. Watts (University of Toronto, Toronto, Canada). MCMV (Smith strain) preparation, injection, and plaque assay were performed as previously described (39).

ELISAs. Mouse IFN-α was determined by sandwich ELISA. In brief, 96-well microtiter plates were coated overnight at 4°C with 5 µg/ml of rat anti-mouse IFN-α antibody (RMMA-1; PBL Biomedical Laboratories) diluted in 0.1 M of sodium carbonate buffer. Wells were blocked for 1 h with PBS/10% FBS and incubated for 2 h with samples or a recombinant mouse IFN-α standard (Sigma-Aldrich). IFN-α was detected with 100 ng/ml of polyclonal rabbit anti-mouse IFN-α antibody (PBL Biomedical Laboratories) for 24 h at room temperature, washed, and incubated for 1 h with a donkey anti-rabbit IgG conjugated to horseradish peroxidase (GE Healthcare), followed by 20 min in 3,3',5,5'-tetramethylbenzidine substrate (Sigma-Aldrich), and 1 M H_2SO_4 was added to stop the reaction. Between incubations, plates were washed three times with PBS/0.05% Tween-20. Optical density was read at 450 nm with a microtiter plate reader (MDS Analytical Technologies). IL-12p70, IL-6, and TNF-α production by pDCs was assayed using commercial ELISA kits (BD).

Immunofluorescence and FACS analysis. The following FACS mAbs were used: biotin-440c (anti-Siglec-H; Cell Sciences), allophycocyanin-mPDCA-1 (anti-BST2; Miltenyi Biotec), FITC-CD86, 2E6 (anti-Ly49Q; eBioscience), allophycocyanin-B220, PE-CD11c, and streptavidin-PE were purchased from BD. NS-34 (anti-Ly49Q) was prepared as previously described (10). PE-conjugated H-$2K^b$/OVA tetramer contains human β2 microglobulin and was purchased from Beckman Coulter. For all FACS analyses, cells were first washed in FACS buffer (PBS, 0.5% BSA, 0.02% NaN_3), and were then incubated for 20 min at 4°C with fluorochrome-conjugated antibodies. Two-step staining involved an additional incubation for 20 min with the appropriate secondary antibody at 4°C, followed by a wash in FACS buffer. Stained cells were analyzed with a flow cytometer (FACSCalibur; BD). Three-color immunofluorescent staining with biotin-rat anti-mPDCA-1 plus streptavidin-Alexa Fluor 594, hamster anti-CD3ε (BD) plus Alexa Fluor 647–goat anti-hamster IgG (Invitrogen), and FITC–anti-CD19 (BD) was performed on slide-mounted 10-µm spleen sections from untreated and CpG-ODN–injected mice. Slides were viewed on a confocal microscope (Axiovert 100M; Car Zeiss, Inc.).

Giemsa staining. Fresh or CpG-ODN–cultured pDCs were cytocentrifuged onto glass slides, fixed in methanol for 10 min, and air dried. Slides were stained with modified Giemsa stain solution (Sigma-Aldrich) diluted 1:10 in distilled H_2O for 10 min, rinsed with distilled H_2O, and mounted. Pictures were obtained with a microscope (Axiophot; Carl Zeiss, Inc.).

Statistical analysis. Unless otherwise indicated, all P values were calculated with the two-tailed Student's *t* test.

We thank Dr. P. Liu for assistance with BAC recombineering; Dr. Q. Zhu for ES cell selection and blastocyst injections; Drs. S.K. Anderson and A. Veillette for helpful discussion; Drs. J. Carlyle, W.-K. Suh, J. Di Noia, and J.-F. Cote for critical reading of the manuscript; and E. Massicotte and M. Dupuis for cell sorting.

This work was supported by an operating grant (MOP 62841) from the Canadian Institutes of Health Research (CIHR). L-H. Tai is supported by a CIHR Cancer Training Program scholarship. S. Belanger is supported by a Fonds de la recherche en santé Québec scholarship. A.P. Makrigiannis is supported by a New Investigator Award from the CIHR.

The authors have no conflicting financial interests.

Submitted: 4 April 2008
Accepted: 14 November 2008

REFERENCES

1. Liu, Y.J. 2005. IPC: professional type 1 interferon-producing cells and plasmacytoid dendritic cell precursors. *Annu. Rev. Immunol.* 23:275–306.
2. Facchetti, F., C. Wolf-Peeters, D.Y. Mason, K. Pulford, J.J. van den Oord, and V.J. Desnet. 1988. Plasmacytoid T cells. Immunohistochemical evidence for their monocyte/macrophage origin. *Am. J. Pathol.* 133:15–21.
3. Abb, J., H. Abb, and F. Deinhardt. 1984. Relationship between natural killer (NK) cells and interferon (IFN) alpha-producing cells in human peripheral blood. Studies with a monoclonal antibody with specificity for human natural killer cells. *Immunobiology.* 167:359–364.
4. Perussia, B., V. Fanning, and G. Trinchieri. 1985. A leukocyte subset bearing HLA-DR antigens is responsible for in vitro alpha interferon production in response to viruses. *Nat. Immun. Cell Growth Regul.* 4:120–137.
5. Kadowaki, N., S. Ho, S. Antonenko, R.W. Malefyt, R.A. Kastelein, F. Bazan, and Y.J. Liu. 2001. Subsets of human dendritic cell precursors express different Toll-like receptors and respond to different microbial antigens. *J. Exp. Med.* 194:863–869.
6. Asselin-Paturel, C., G. Brizard, J.J. Pin, F. Briere, and G. Trinchieri. 2003. Mouse strain differences in plasmacytoid dendritic cell frequency and function revealed by a novel monoclonal antibody. *J. Immunol.* 171: 6466–6477.
7. Nakano, H., M. Yanagita, and M.D. Gunn. 2001. CD11c$^+$B220$^+$Gr-1$^+$ cells in mouse lymph nodes and spleen display characteristics of plasmacytoid dendritic cells. *J. Exp. Med.* 194:1171–1178.
8. Asselin-Paturel, C., A. Boonstra, M. Dalod, I. Durand, N. Yessaad, C. Dezutter-Dambuyant, A. Vicari, A. O'Garra, C. Biron, F. Briere, and G. Trinchieri. 2001. Mouse type I IFN-producing cells are immature APCs with plasmacytoid morphology. *Nat. Immunol.* 2:1144–1150.
9. Blasius, A., W. Vermi, A. Krug, F. Facchetti, M. Cella, and M. Colonna. 2004. A cell-surface molecule selectively expressed on murine natural interferon-producing cells that blocks secretion of interferon-alpha. *Blood.* 103:4201–4206.
10. Toyama-Sorimachi, N., Y. Tsujimura, M. Maruya, A. Onoda, T. Kubota, S. Koyasu, K. Inaba, and H. Karasuyama. 2004. Ly49Q, a member of the Ly49 family that is selectively expressed on myeloid lineage cells and involved in regulation of cytoskeletal architecture. *Proc. Natl. Acad. Sci. USA.* 101:1016–1021.
11. Kamogawa-Schifter, Y., J. Ohkawa, S. Namiki, N. Arai, K. Arai, and Y. Liu. 2005. Ly49Q defines 2 pDC subsets in mice. *Blood.* 105:2787–2792.
12. Blasius, A.L., M. Cella, J. Maldonado, T. Takai, and M. Colonna. 2006. Siglec-H is an IPC-specific receptor that modulates type I IFN secretion through DAP12. *Blood.* 107:2474–2476.
13. Blasius, A.L., E. Giurisato, M. Cella, R.D. Schreiber, A.S. Shaw, and M. Colonna. 2006. Bone marrow stromal cell antigen 2 is a specific marker of type I IFN-producing cells in the naive mouse, but a promiscuous cell surface antigen following IFN stimulation. *J. Immunol.* 177:3260–3265.
14. Wilhelm, B.T., L. Gagnier, and D.L. Mager. 2002. Sequence analysis of the Ly49 cluster in C57BL/6 mice: a rapidly evolving multigene family in the immune system. *Genomics.* 80:646–661.
15. Makrigiannis, A.P., A.T. Pau, P.L. Schwartzberg, D.W. McVicar, T.W. Beck, and S.K. Anderson. 2002. A BAC contig map of the Ly49 gene cluster in 129 mice reveals extensive differences in gene content relative to C57BL/6 mice. *Genomics.* 79:437–444.
16. Proteau, M.-F., E. Rousselle, and A.P. Makrigiannis. 2004. Mapping of the BALB/c Ly49 cluster defines a minimal natural killer cell receptor gene repertoire. *Genomics.* 84:669–677.
17. Toyama-Sorimachi, N., Y. Omatsu, A. Onoda, Y. Tsujimura, T. Iyoda, A. Kikuchi-Maki, H. Sorimachi, T. Dohi, S. Taki, K. Inaba, and H. Karasuyama. 2005. Inhibitory NK receptor Ly49Q is expressed on subsets of dendritic cells in a cellular maturation- and cytokine stimulation-dependent manner. *J. Immunol.* 174:4621–4629.
18. Makrigiannis, A.P., D. Patel, M.L. Goulet, K. Dewar, and S.K. Anderson. 2005. Direct sequence comparison of two divergent class I MHC natural killer cell receptor haplotypes. *Genes Immun.* 6:71–83.
19. Omatsu, Y., T. Iyoda, Y. Kimura, A. Maki, M. Ishimori, N. Toyama-Sorimachi, and K. Inaba. 2005. Development of murine plasmacytoid dendritic cells defined by increased expression of an inhibitory NK receptor, Ly49Q. *J. Immunol.* 174:6657–6662.

20. Colonna, M., G. Trinchieri, and Y.J. Liu. 2004. Plasmacytoid dendritic cells in immunity. *Nat. Immunol.* 5:1219–1226.
21. Tai, L.H., M.L. Goulet, S. Belanger, A.D. Troke, A.G. St Laurent, A. Mesci, N. Toyama-Sorimachi, J.R. Carlyle, and A.P. Makrigiannis. 2007. Recognition of H-2K(b) by Ly49Q suggests a role for class Ia MHC regulation of plasmacytoid dendritic cell function. *Mol. Immunol.* 44:2638–2646.
22. Fuchs, A., M. Cella, T. Kondo, and M. Colonna. 2005. Paradoxic inhibition of human natural interferon-producing cells by the activating receptor NKp44. *Blood.* 106:2076–2082.
23. Asselin-Paturel, C., G. Brizard, K. Chemin, A. Boonstra, A. O'Garra, A. Vicari, and G. Trinchieri. 2005. Type I interferon dependence of plasmacytoid dendritic cell activation and migration. *J. Exp. Med.* 201:1157–1167.
24. Krug, A., A.R. French, W. Barchet, J.A. Fischer, A. Dzionek, J.T. Pingel, M.M. Orihuela, S. Akira, W.M. Yokoyama, and M. Colonna. 2004. TLR9-dependent recognition of MCMV by IPC and DC generates coordinated cytokine responses that activate antiviral NK cell function. *Immunity.* 21:107–119.
25. Tabeta, K., P. Georgel, E. Janssen, X. Du, K. Hoebe, K. Crozat, S. Mudd, L. Shamel, S. Sovath, J. Goode, et al. 2004. Toll-like receptors 9 and 3 as essential components of innate immune defense against mouse cytomegalovirus infection. *Proc. Natl. Acad. Sci. USA.* 101:3516–3521.
26. Lee, S.H., J. Gitas, A. Zafer, P. Lepage, T.J. Hudson, A. Belouchi, and S.M. Vidal. 2001. Haplotype mapping indicates two independent origins for the Cmv1s susceptibility allele to cytomegalovirus infection and refines its localization within the Ly49 cluster. *Immunogenetics.* 53:501–505.
27. Lee, S.H., S. Girard, D. Macina, M. Busa, A. Zafer, A. Belouchi, P. Gros, and S.M. Vidal. 2001. Susceptibility to mouse cytomegalovirus is associated with deletion of an activating natural killer cell receptor of the C-type lectin superfamily. *Nat. Genet.* 28:42–45.
28. Brown, M.G., A.O. Dokun, J.W. Heusel, H.R. Smith, D.L. Beckman, E.A. Blattenberger, C.E. Dubbelde, L.R. Stone, A.A. Scalzo, and W.M. Yokoyama. 2001. Vital involvement of a natural killer cell activation receptor in resistance to viral infection. *Science.* 292:934–937.
29. Nakamura, M.C., E.C. Niemi, M.J. Fisher, L.D. Shultz, W.E. Seaman, and J.C. Ryan. 1997. Mouse Ly-49A interrupts early signaling events in natural killer cell cytotoxicity and functionally associates with the SHP-1 tyrosine phosphatase. *J. Exp. Med.* 185:673–684.
30. Mason, L.H., J. Willette-Brown, A.T. Mason, D. McVicar, and J.R. Ortaldo. 2000. Interaction of Ly-49D+ NK cells with H-2Dd target cells leads to Dap-12 phosphorylation and IFN-gamma secretion. *J. Immunol.* 164:603–611.
31. Sjolin, H., S.H. Robbins, G. Bessou, A. Hidmark, E. Tomasello, M. Johansson, H. Hall, F. Charifi, G.B. Karlsson Hedestam, C.A. Biron, et al. 2006. DAP12 signaling regulates plasmacytoid dendritic cell homeostasis and down-modulates their function during viral infection. *J. Immunol.* 177:2908–2916.
32. Hamerman, J.A., N.K. Tchao, C.A. Lowell, and L.L. Lanier. 2005. Enhanced Toll-like receptor responses in the absence of signaling adaptor DAP12. *Nat. Immunol.* 6:579–586.
33. Hamerman, J.A., J.R. Jarjoura, M.B. Humphrey, M.C. Nakamura, W.E. Seaman, and L.L. Lanier. 2006. Cutting edge: inhibition of TLR and FcR responses in macrophages by triggering receptor expressed on myeloid cells (TREM)-2 and DAP12. *J. Immunol.* 177:2051–2055.
34. Kim, S., J. Poursine-Laurent, S.M. Truscott, L. Lybarger, Y.J. Song, L. Yang, A.R. French, J.B. Sunwoo, S. Lemieux, T.H. Hansen, and W.M. Yokoyama. 2005. Licensing of natural killer cells by host major histocompatibility complex class I molecules. *Nature.* 436:709–713.
35. Fernandez, N.C., E. Treiner, R.E. Vance, A.M. Jamieson, S. Lemieux, and D.H. Raulet. 2005. A subset of natural killer cells achieves self-tolerance without expressing inhibitory receptors specific for self-MHC molecules. *Blood.* 105:4416–4423.
36. Muller, U., U. Steinhoff, L.F. Reis, S. Hemmi, J. Pavlovic, R.M. Zinkernagel, and M. Aguet. 1994. Functional role of type I and type II interferons in antiviral defense. *Science.* 264:1918–1921.
37. Liu, P., N.A. Jenkins, and N.G. Copeland. 2003. A highly efficient recombineering-based method for generating conditional knockout mutations. *Genome Res.* 13:476–484.
38. Makrigiannis, A.P., A.T. Pau, A. Saleh, R. Winkler-Pickett, J.R. Ortaldo, and S.K. Anderson. 2001. Class I MHC-binding characteristics of the 129/J Ly49 repertoire. *J. Immunol.* 166:5034–5043.
39. Desrosiers, M.P., A. Kielczewska, J.C. Loredo-Osti, S.G. Adam, A.P. Makrigiannis, S. Lemieux, T. Pham, M.B. Lodoen, K. Morgan, L.L. Lanier, and S.M. Vidal. 2005. Epistasis between mouse Klra and major histocompatibility complex class I loci is associated with a new mechanism of natural killer cell-mediated innate resistance to cytomegalovirus infection. *Nat. Genet.* 37:593–599.

Genes and Immunity (2008) 9, 214–223

www.nature.com/gene

ORIGINAL ARTICLE

Association of LILRA2 (ILT1, LIR7) splice site polymorphism with systemic lupus erythematosus and microscopic polyangiitis

K Mamegano[1,8], K Kuroki[2,8], R Miyashita[1], M Kusaoi[3], S Kobayashi[3], K Matsuta[4], K Maenaka[2], M Colonna[5], S Ozaki[6], H Hashimoto[3], Y Takasaki[3], K Tokunaga[1] and N Tsuchiya[7]

[1]*Department of Human Genetics, Graduate School of Medicine, The University of Tokyo, Tokyo, Japan;* [2]*Division of Structural Biology, Medical Institute of Bioregulation, Kyushu University, Fukuoka, Japan;* [3]*Department of Rheumatology and Internal Medicine, Juntendo University, Tokyo, Japan;* [4]*Matsuta Clinic, Tokyo, Japan;* [5]*Division of Biology and Biomedical Science, Washington University, St Louis, MO, USA;* [6]*Department of Internal Medicine, St Marianna University School of Medicine, Kawasaki, Japan and* [7]*Doctoral Program in Social and Environmental Medicine, Graduate School of Comprehensive Human Sciences, University of Tsukuba, Tsukuba, Japan*

Leukocyte immunoglobulin-like receptors (LILRs) are inhibitory, stimulatory or soluble receptors encoded within the leukocyte receptor complex. Some LILRs are extensively polymorphic, and exhibit evidence for balancing selection and association with disease susceptibility. LILRA2 (LIR7/ILT1) is an activating receptor highly expressed in inflammatory tissues, and is involved in granulocyte and macrophage activation. In this study, we examined the association of LILRA2 and adjacently located LILRA1 with systemic lupus erythematosus (SLE), rheumatoid arthritis (RA) and microscopic polyangiitis (MPA). Polymorphism screening detected a LILRA2 SNP (rs2241524 G>A) that disrupts splice acceptor site of intron 6. Case–control association studies on 273 Japanese SLE, 296 RA, 50 MPA and 284 healthy individuals revealed increase of genotype A/A in SLE (12.1%, odds ratio (OR) 1.82, 95% confidence interval (CI) 1.02–3.24, P = 0.041) and in MPA (16.0%, OR 2.52, 95% CI 1.07–5.96, P = 0.049) compared with healthy individuals (7.0%). The risk allele caused an activation of a cryptic splice acceptor site that would lead to a novel LILRA2 isoform lacking three amino acids in the linker region (Δ419–421). Flow cytometry indicated that this isoform was expressed on the surface of monocytes. These findings suggested that LILRA2 Δ419–421 isoform encoded by the splice site SNP may play a role in SLE and MPA.

Genes and Immunity (2008) 9, 214–223; doi:10.1038/gene.2008.5; published online 14 February 2008

Keywords: *LILRA2; splice acceptor site; polymorphism; systemic lupus erythematosus; microscopic polyangiitis*

Introduction

The family of leukocyte immunoglobulin (Ig)-like receptor (LILR, also known as LIR, immunoglobulin-like transcript (ILT), CD85 or monocyte/macrophage inhibitory receptor) consists of 13 member genes including two pseudogenes (LILRP1 and LILRP2).[1–3] LILRs can be divided into three groups. The first group (LILRA1, -A2, -A4, -A5 and -A6) delivers positive signals by pairing with the Fc receptor common γ-chain (FcRγ), which contains an immunoreceptor tyrosine-based activation motif. The second (LILRB1, -B2, -B3, -B4 and -B5) contains 2–4 immunoreceptor tyrosine-based inhibitory motif-like sequences within the cytoplasmic region and inhibits cell activation by recruiting Src homology 2 (SH2)-containing tyrosine phosphatase-1 (SHP-1) or SH2 domain-containing inositol phosphatase (SHIP). The third group, LILRA3 and LILRA5s, is thought to be secreted as soluble receptors.

The *LILR* gene family is located in the leukocyte receptor complex on human chromosome 19q13.4, which also contains a number of closely related Ig-like receptor genes such as killer cell Ig-like receptors (*KIRs*) and *FCAR*.[4–6] This region has been suggested to be one of the candidate susceptibility regions for systemic lupus erythematosus (SLE) by linkage analyses.[7,8] In the syntenic region of mice, proximal end of chromosome 7, activating and inhibitory paired Ig-like receptor A and B (*Pira, Pirb*), orthologs of human *LILR* genes, are located.[9,10] Mice lacking *Pirb* showed impaired maturation of dendritic cells (DCs) and increased Th2 responses.[11] Furthermore, it was reported that both PIR-A and -B proteins bind to various mouse MHC class I molecules, and *Pirb*-deficient mice showed exacerbated graft-versus-host disease.[12] These observations suggest that LILRs may be critically involved in the regulation of immune system in various aspects.

LILRA2 is an activation receptor broadly expressed on hematopoietic cells such as monocytes, macrophages, myeloid DCs, granulocytes and subset of NK cells.[13,14] It

Correspondence: Professor N Tsuchiya, Doctoral Program in Social and Environmental Medicine, Graduate School of Comprehensive Human Sciences, University of Tsukuba, 1-1-1 Tennodai, Tsukuba, Ibaraki 305-8575, Japan.
E-mail: tsuchiya@md.tsukuba.ac.jp
[8]These two authors equally contributed to this work.
Received 6 September 2007; revised 17 January 2008; accepted 17 January 2008; published online 14 February 2008

is reported that the expression of LILRA2 was significantly upregulated in lesions of lepromatous leprosy patients.[15] The synovium from patients with rheumatoid arthritis (RA) showed extensive expression of inhibitory LILRB2 and activating LILRA2 on macrophages and neutrophils.[16] Although some of the LILRs and KIRs bind to HLA class I molecules or UL-18, a HLA class I homolog expressed by human cytomegalovirus,[17,18] ligands for LILRA2 have not been identified.

LILRA2 is implicated in the activation of eosinophils,[19] basophils[20] and macrophages.[21] On the other hand, it is reported that activation of LILRA2 suppresses innate host defense mechanisms by shifting monocyte production from IL-12 toward IL-10 and blocking toll-like receptor (TLR)-mediated antimicrobial activity.[15] In mice, PIR-A, an ortholog of LILRA2, has been shown to be an essential costimulatory receptor for osteoclast differentiation.[22]

RA is a chronic rheumatic disease that leads to progressive joint destruction. It is characterized by synovial proliferation and autoimmune features such as production of rheumatoid factor and anticyclic citrullinated peptide antibodies. SLE is a prototypic systemic autoimmune disease characterized by multisystem organ involvement, high level of antinuclear autoantibody and immune complex deposition. Microscopic polyangiitis (MPA) is a rare disease characterized by necrotizing vasculitis of small-to-medium-size vessels, and the patients often present with severe manifestations such as rapidly progressive glomerulonephritis and pulmonary hemorrhage. Most of the patients with MPA exhibit antineutrophil cytoplasmic antibodies. The etiology of these rheumatic diseases is poorly understood, but probably involves interactions among environmental and genetic factors.

We have been interested in the role of diversity of immunoregulatory molecules in the genetic background of human rheumatic diseases, and Ig-like receptor superfamily has been one of our major targets.[23–25] With respect to the LILR family, we thus far reported that *LILRB1* was highly polymorphic and associated with susceptibility to RA.[26] Extensive polymorphism appears to be a feature of LILR family, and evidence for balancing selection has been found for another activating member of LILR family, *LILRA3*.[27]

As described above, human chromosome 19q13 has been suggested to be one of the candidate loci for susceptibility to SLE. LILRA2 is functionally implicated in immunoregulation, granulocyte activation and potentially osteoclast differentiation. These constitute crucial pathways of the rheumatic diseases such as SLE, RA and MPA. In this study, we examined whether *LILRA2* polymorphisms are associated with susceptibility to human SLE, RA and MPA.

Results

Association of a LILRA2 *splice acceptor site polymorphism with susceptibility to SLE*

Polymorphism screening of all exons and promoter region (approximately 2 kb) of *LILRA2* gene was performed on genomic DNA from 12 Japanese SLE, 12 RA patients and 16 Japanese controls by direct sequencing. Six single nucleotide polymorphisms (SNPs) and three rare variations (only one heterozygote among all individuals screened) were detected (Figure 1).

Among the detected SNPs, rs2241524 (IVS6-1 G>A) located at intron 6–exon 7 junction disrupts the consensus splicing acceptor motif and was thought to be functionally relevant. Case–control association study demonstrated that A/A genotype was increased in SLE (odds ratio (OR) 1.82, 95% confidence interval (CI) 1.02–3.24, $P = 0.041$) as compared with controls (Table 1). The control genotype was not deviated from Hardy–Weinberg equilibrium. The genotype frequency in the controls was similar to that of Japanese sample set in the HapMap database (http://www.hapmap.org/index.html.en) (G/G 51.2%, G/A 44.2%, A/A 4.7%). Actually, the increase in the A/A genotype in the patients was even more striking when compared with the HapMap samples, because the frequency of A/A was slightly lower in the HapMap samples than in our controls.

Lack of association of other polymorphisms in the linkage disequilibrium block encompassing rs2241524

We next investigated whether this association might be caused by linkage disequilibrium (LD) with other causative variations. According to the HapMap database, the LD block encompassing rs2241524 contains the entire *LILRA2* locus and 5′ portion of adjacently located *LILRA1* (*LIR6*) locus, and no other gene was present. We carried out polymorphism screening of *LILRA1* including the promoter region (approximately 1.4 kb). Twenty-four *LILRA1* SNPs, including 11 novel SNPs, were identified (Figure 1). Among these, 5′ portion 19 SNPs (from promoter region to intron 7) were found to constitute two major haplotypes, tentatively designated *LILRA1.PC01* and *LILRA1.PC02* (PC stands for promoter and coding region) (Table 2a, Figure 1). The frequency of *LILRA1.PC01* was 74.2% and that of *LILRA1.PC02* was 22.6% in the parents of 31 Japanese healthy samples used for haplotype determination, whereas c.490C>T (H164Y) and c.581C>G (S194W) seemed to be infrequent variations (<1%).

We next examined association of potentially functional *LILRA2* polymorphisms in the promoter region (rs3760856, rs28384501, rs28384502) and also *LILRA1.PC* haplotype with SLE. rs28384501 and rs28384502 were only 2 bp apart and in absolute LD in the controls used in this study. Other polymorphic sites were also in significant, but not absolute LD (Figure 1). None of these polymorphisms was significantly associated with SLE, nor haplotypes were formed by these polymorphic sites (Tables 2b and c). Thus, we concluded that *LILRA2* rs2241524 itself was most likely to be responsible for the association with SLE.

Association of a LILRA2 *rs2241524 with susceptibility to MPA*

We next examined whether *LILRA2* rs2241524 was associated with RA and MPA. Association of A/A genotype was observed in MPA (OR 2.52, 95% CI 1.07–5.96, $P = 0.049$), but not in RA (Table 1).

Effects of the LILRA2 *splice acceptor SNP on the transcript*

Because rs2241524 disrupts the consensus splicing acceptor motif of *LILRA2* intron 6, we investigated the difference in the sequence of mRNA generated from each allele. To detect a small difference in mRNA size,

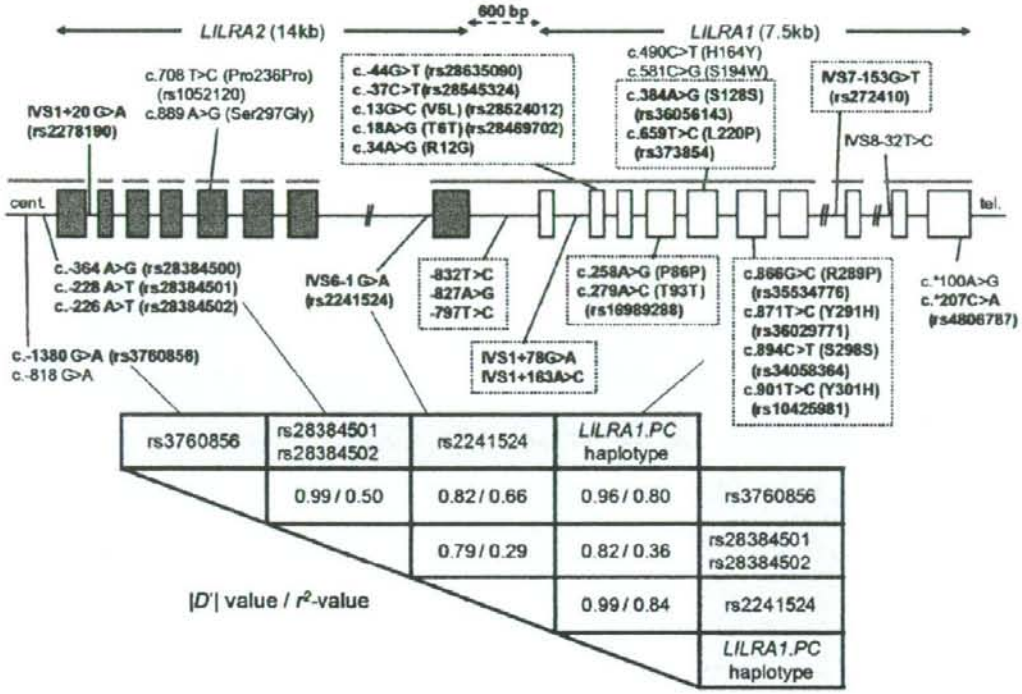

Figure 1 Genomic configuration of *LILRA1*, *LILRA2* and variations detected in Japanese. Boxes indicate exons. The variations shown in bold are polymorphisms, and others are rare variations. The size of each exon and intron is not to scale. The regions screened in this study are shown as gray lines. *LILRA1* single nucleotide polymorphisms (SNPs) boxed in dotted lines constitute two major haplotypes (*LILRA1.PC01* and *LILRA1.PC02*). Pairwise linkage disequilibrium (LD) parameters in *LILRA2* polymorphisms and *LILRA1* haplotypes are shown in lower column. Moderate-to-strong LD was observed between polymorphic sites. Absolute LD was observed between rs28384501 and rs2838402, which are 2 bp apart.

Table 1 Frequencies of *LILRA2* splice acceptor site polymorphism in Japanese patients with SLE, RA, MPA and healthy controls

LILRA2 *rs2241524*	*SLE (%)* n = 273	*RA (%)* n = 290	*MPA (%)* n = 50	*Controls (%)* n = 285
Genotype frequency				
G/G	142 (52.0)	151 (52.1)	22 (44.0)	153 (53.7)
G/A	98 (35.9)	111 (38.3)	20 (40.0)	112 (39.3)
A/A	33 (12.1)[a]	28 (9.6)	8 (16.0)[b]	20 (7.0)
Allele frequency				
G	382 (70.0)	413 (71.2)	64 (64.0)	418 (73.3)
A	164 (30.0)	167 (28.8)	36 (36.0)	152 (26.7)

Abbreviations: MPA, microscopic polyangiitis; RA, rheumatoid arthritis; SLE, systemic lupus erythematosus.
[a]SLE versus control: A/A versus (G/A+G/G): OR 1.82, 95% CI 1.02–3.24, $P = 0.041$ (χ^2-test).
[b]MPA versus control: A/A versus (G/A+G/G): OR 2.52, 95% CI 1.07–5.96, $P = 0.049$ (Fischer's exact test).

RT–PCR was performed using primers placed on exon 6 and 7, and the products were analyzed by capillary gel electrophoresis. This analysis revealed a clear difference in size of the mRNA from each allele (Figure 2a).

By sequencing, the longer product derived from G allele was found to be conventional *LILRA2* transcript, whereas the band derived from A allele was found to encode a 9-nucleotide shorter novel transcript. This isoform was caused by the activation of a cryptic splice acceptor site 9-nt downstream to the original site (Figure 2b). The usage of the alternative splice acceptor site was absolutely dependent on the genotype, because only a single product, long and short, was amplified from G/G and A/A genotypes, respectively (Figure 2a).

Such alternative splicing was presumed to result in the deletion of three amino acids (Ala-Ser-Leu at position 419–421) in the linker region between Ig-like domains and transmembrane region of LILRA2 protein (Figure 2c). This isoform was termed as Δ419–421 isoform.

Cell surface expression of LILRA2 isoforms

We next examined whether the Δ419–421 isoform was expressed at the protein level. Because peripheral blood monocytes are known to express LILRA2, two-color flow cytometric analysis was performed using monoclonal antibodies (mAbs) against LILRA2 (anti-ILT1 mAb135)[14] and CD14. This analysis was performed using two healthy donors with G/G and two with A/A genotype.

LILRA2 was detected on the monocytes both from G/G and A/A donors (Figure 3). Because individuals with A/A genotype exclusively use the cryptic splice site, detection of LILRA2 protein on the cell surface in

Table 2 Association of *LILRA2* rs2241524 is not caused by LD with other polymorphisms

(a) Haplotype constituting 5′ portion of LILRA1 locus

Position[a]	*−832*	*−827*	*−797*	*IVS1+78*	*IVS1+163*	*c.−44*	*c.−37*	*c.13*	*c.18*	*c.34*	*c.258*	*c.279*	*c.384*	*c.659*	*c.866*	*c.871*	*c.894*	*c.901*	*IVS7-153*
LILRA1.PC01	T	A	T	G	A	G	C	G	A	A	A	A	A	T	G	T	C	T	T
LILRA1.PC02	C	G	C	A	C	T	T	C	G	G	G	C	G	C	C	C	T	C	G

(b) Lack of association of other polymorphic sites in the LD block encompassing LILRA2 rs2241524

Polymorphic site	*Minor allele (2)*	*SLE (%)*			*Healthy controls (%)*			*Recessive model*[b]		
		1/1	*1/2*	*2/2*	*1/1*	*1/2*	*2/2*	*OR*	*95% CI*	P
rs3760856 G>A	A	52.0	35.9	12.1	52.1	38.3	9.6	1.35	0.76–2.40	0.30
rs28384501 A>T[c]	T	29.5	47.7	22.8	29.9	48.8	21.3	1.09	0.73–1.63	0.69
LILRA1.PC	02	50.7	36.1	13.2	48.4	42.2	9.4	1.45	0.85–2.48	0.17

(c) Frequencies of LILRA2–LILRA1 region haplotypes in Japanese patients with SLE and controls

Haplotype	*LILRA2*	*LILRA2*	*LILRA2*	*LILRA1.PC*	*Haplotype frequency (%)*	
	rs3760856	*rs28384501*	*rs2241524*		*SLE*	*Healthy controls*
A	G	A	G	01	50.0	50.3
B	A	T	A	02	26.8	24.3
C	G	T	G	01	18.5	17.7
D	G	A	A	02	2.8	3.4

Abbreviations: CI, confidence interval; LD, linkage disequilibrium; OR, odds ratio; SLE, systemic lupus erythematosus.
[a]Numbering starts at the ATG translation initiation codon. rs number for each SNP is shown in Figure 1.
[b]Association was shown under the recessive model, because the association of rs2241524 was detected under this model. Other models also failed to detect significant association.
[c]*LILRA2* rs28384501 A>T is in absolute LD with rs28384502 A>T.

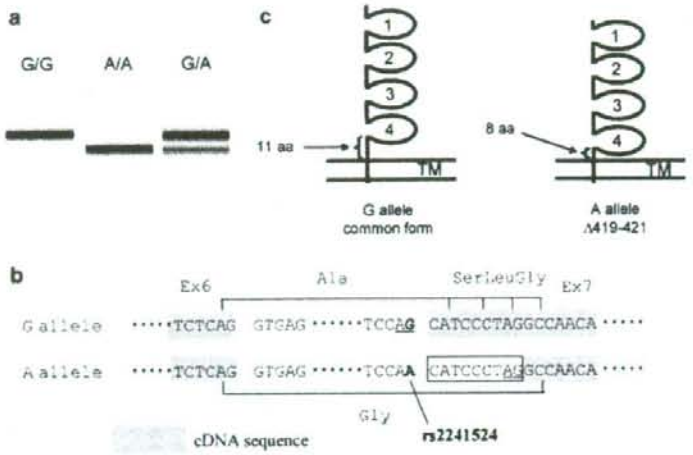

Figure 2 *LILRA2* splice acceptor site single nucleotide polymorphism (SNP) rs2241524 activates a cryptic splice acceptor site and causes in-frame deletion of three amino acid in the linker region. (**a**) Capillary electrophoresis of reverse transcriptase (RT)–PCR products from individuals with each genotype revealed two fragments of different sizes that were completely segregated according to the genotype. (**b**) DNA sequencing revealed that G-allele transcript employs a cryptic splice acceptor site. This results in the deletion of 9 nucleotides (9-nt) (open box) that leads to in-frame deletion of three amino acids. The splice acceptor site used by each allele is shown by underline. (**c**) The deletion of three amino acids in the LILRA2 protein product from G allele leads to shortening of the linker region.

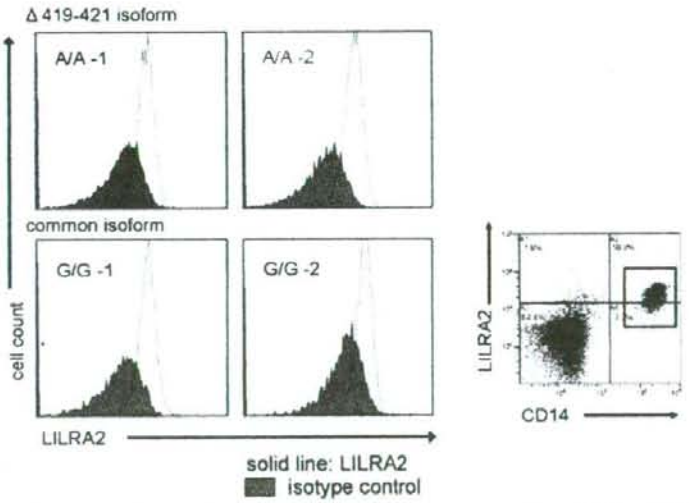

Figure 3 Δ419–421 isoform is expressed on the CD14+ peripheral blood mononuclear cells (PBMCs). PBMCs from individuals with rs2241524 A/A or G/G genotype were double-stained with anti-LILRA2 mAb and anti-CD14. The expression of LILRA2 was mainly observed in the CD14+ monocytes (right panel). Surface expression of LILRA2 protein was detected on monocytes similarly in donors with G/G and A/A genotypes, indicating that Δ419–421 isoform is expressed on the surface of monocytes (left panels).

these donors indicated that LILRA2 Δ419–421 protein isoform was expressed on the cell surface. The intensity of LILRA2 staining was similar in both genotypes.

Discussion

In this study, we reported evidence that suggests association of an intron 6–exon 7 junction SNP of *LILRA2* with susceptibility to SLE and MPA. This SNP disrupts the consensus splice acceptor motif, and results in the activation of a cryptic splice acceptor site located at 9-nt downstream to the original site, leading to the in-frame deletion of three amino acids in the linker region of LILRA2 protein (Δ419–421). The usage of the alternative splice acceptor site was entirely dependent on the genotype; thus, G allele always gives rise to the common isoform, while A allele exclusively produces Δ419–421

transcripts. The presence of LILRA2 protein on the surface of monocytes from A/A genotype, therefore, indicates that the Δ419–421 isoform is expressed on the cell surface at the protein level.

The mechanism of association of LILRA2 remains speculative. The signal intensity of LILRA2 in the flow cytometric analysis did not substantially differ between individuals with G/G and A/A genotypes, suggesting that Δ419–421 did not affect expression level or gross structure of the protein. It would be more likely that the deletion of the three amino acids alters affinity of the LILRA2 to as yet unknown ligands and/or FcRγ chain, which is the signaling component of LILRA2.

It has been shown that LILRA2 modifies TLR signaling in monocytes and macrophages.[15] A number of recent observations demonstrate the crucial role of type I interferon in SLE.[28] Because TLR signals are important inducers of type I interferons, association with SLE could be explained if Δ419–421 isoform may promote stronger TLR signals.

In MPA, activation of neutrophils and macrophages plays an important role in the pathogenesis.[29] Several lines of evidence demonstrated the role of LILRA2 in the activation of myeloid cells and macrophages.[14,19–21] Thus, stronger signals via Δ419–421 isoform might explain its association with MPA.

LILRA2 was also suggested to play a role in the regulation of Th1/Th2 balance.[15] As Th1 cytokines have been implicated both in SLE and MPA,[29,30] Th1/Th2 imbalance caused by Δ419–421 isoform could be another potential mechanism of association. The association of *LILRA2* was in a recessive manner, which was responsible for the deviation of this genotype from the Hardy–Weinberg equilibrium in SLE. Such recessive association could suggest a loss-of-function mechanism. If *LILRA2* Δ419–421 isoform is associated with reduced induction of Th2 cytokines and leads to Th1-dominant environment, the recessive mode of genetic association might be explained.

The power to detect susceptibility genes in this study was not sufficient in the case of MPA due to its rarity. Assuming that prevalence of SLE, RA and MPA is 0.001, 0.01 and 0.0001, respectively, and the population frequency of the risk allele is 0.25, the power to detect susceptibility genes with the genotype relative risk of 1.5 at the significance level of 0.05 is calculated to be 0.87, 0.88 and 0.42, respectively.[31] In addition, because the *P*-values are marginal, genotyping error could lead to false positive association. However, such a possibility is unlikely; the genotyping was performed by direct sequencing and the genotyping error rate should be negligible. Furthermore, the frequency of the A/A genotype in the Japanese samples on the HapMap database was even lower compared with our controls, which lend support to the association of this genotype with SLE and MPA. Nevertheless, in order to confirm this association, independent studies in Japanese and other populations should be performed in the future. Another limitation of this study was a bias in the sex ratio between cases and controls. However, because the frequency of each SNP was not significantly different between males and females, the results were essentially identical when they are adjusted for the sex ratio.

In conclusion, this study suggested that the splice acceptor site polymorphism of *LILRA2* leading to the deletion of three amino acids was associated with susceptibility to SLE and MPA in Japanese. Taken together with the previous observations from our laboratory, LILR family members are rich in functional polymorphisms, and may be involved in the genetic background of immune response diversity in the human population as well as in the susceptibility to multiple immune system disorders.

Patients and methods

Patients and controls

A total of 273 patients with SLE (male 17, female 256, mean age ± s.d. 41.3 ± 13.5) and 290 patients with RA (male 30, female 260, mean age ± s.d. 58.9 ± 11.5) were recruited from Matsuta Clinic, Juntendo University Hospital and the University of Tokyo Hospital. A total of 50 patients with MPA (male 19, female 31, mean age ± s.d. 63.3 ± 13.5) participated in the study at 11 clinical centers in central Japan.[25,32,33] A total of 285 healthy controls (male 164, female 121, mean age ± s.d. 31.7 ± 9.2) were recruited at the University of Tokyo and Japanese Red Cross Blood Centers in Tokyo and Kanagawa. The patients with RA and SLE were diagnosed according to the classification criteria of American College of Rheumatology.[34,35] Classification of vasculitides was essentially based on the definitions of Chapel Hill Conference.[36] Since those definitions do not provide diagnostic or classification criteria, and ACR classification criteria do not include MPA, the MPA was diagnosed in accord with the Japanese criteria proposed by the Research Committee in 1998.[32] This study was approved by the research ethics review committees of the University of Tokyo, University of Tsukuba, Juntendo University and each participating institute.

Genomic DNA from patients and healthy individuals was purified from peripheral blood using the QIAamp blood Kit (Qiagen, Hilden, Germany).

Polymorphism screening and genotyping of LILRA2

Polymorphisms of all exons and promoter region of *LILRA2* gene were screened using PCR-direct sequencing method. Genomic DNA samples from 16 healthy individuals, 12 SLE and 12 RA patients were used for screening. The primers were designed according to the genomic DNA sequence of human *LILRA2* (NCBI accession no. NC_000019). The primers used for polymorphism screening and the regions screened are shown in Table 3 and Figure 1. Because the genomic DNA sequences of *LILR* family genes are highly homologous, nested PCR was used to achieve specific amplification of *LILRA2*. *LILRA2* gene was divided into three fragments. Two fragments of 5′ region (2040 bp upstream from the translation start site to 355 bp downstream of the 3′ end of exon 6) were amplified as overlapping fragments by means of long PCR (nested first PCR) using two primer sets. A fragment encompassing the entire exon 7 was separately amplified. Because intron 6 extends approximately 11 kb, a systematic polymorphism screening was not performed.

As for nested first PCR, one primer set was placed within the promoter region and intron 1 (proNesF–proNesR) (Table 3), and the other was placed within promoter region and intron 6 (NesF–NesR) (Table 3).

Table 3 Primers for PCR-direct sequencing of *LILRA2*

Fragment	*Name*	*Primer*	*Position*
Nested	LILRA2-proNesF	CACGCACCTGACCTTTCATA	Promoter
	LILRB1-proNesR	GAGGGATTTTTCCCCTGAAG	int1
Nested	LILRA2-NesF	CACTTCCTGTGTGGTTGCAC	Promoter
	LILRA2-NesR	GGGGTCAGGACATAGGGTTT	int6
ex1	LILRA2-1F	CACTTCCTGTGTGGTTGCAC	Promoter
	LILRA2-1R	GAGGGATTTTTCCCCTGAAG	int1
ex2	LILRA2-2F	CATCCTCACGGTCCTGATCT	ex1
	LILRA2-2R	CAGCCCAGAACTGCTATTCC	int2
ex3	LILRA2-3F	GAGATCTGTTGGGTGGGAAA	int2
	LILRA2-3R	CCTTCCTGAGGGCAGAGC	int3
ex4	LILRA2-4F	AGCCCCATTTAACACAGTGC	int3
	LILRA2-4R	CTCAGGGAGACTCAGGGAACT	int4
ex5	LILRA2-5F	GTTTGTGGGGAAGCCTGAG	int4
	LILRA2-5R	CCTGGGTCCCTGACTGAAC	int5
ex6	LILRA2-6F	CCCTCACCCATCCTTCTTCT	int5
	LILRA2-6R	GCTCGGAGAGGACAAGATCA	int6
ex7	LILRA2-7F	CCTGGGTGGACATACAGGAG	int6
	LILRA2-7R	AAAAGGGGATCCAGTCAAGG	3′-gene flanking
Promoter	LILRA2-pro1F	AGGTGCGTCTCTGCTGATCT	Promoter
	LILRA2-pro1R	GTGCAACCACACAGGAAGTG	Promoter
Promoter	LILRA2-pro2F	GACGGTTTGGTAGGAAGGAA	Promoter
	LILRA2-pro2R	AGATCAGCAGAGACGCACCT	Promoter
Promoter	LILRA2-pro3F	TGCGTCTCAATGTGAGGAAC	Promoter
	LILRA2-pro3R	CTGATTCTGGGGAAGGTGAG	Promoter
Promoter	LILRA2-TAF	CAACGCTGAGCTGATGGAC	Promoter
	LILRA2-TAR	CAGGACAGAGAGACGCACAG	Promoter
Genotyping	LILRA2-SF	TCAGTTATGGGACTGGCACA	int6
	LILRA2-SR	GGCTGCATCTTGTAGGCTTC	ex7

Abbreviations: ex, exon; int, intron.
These primers were designed according to the genomic DNA sequence of human *LILRA2* (NCBI accession no. NC_000019). These primers were used for nested PCR primers except for LILRA2-SF and -SR, which were used to genotype rs2241524 by a single-step direct sequencing.

Both PCRs were performed in 25 μl reaction mixtures containing 1 μl genomic DNA, 0.4 pM of each primer, 0.4 mM dNTPs, 2 mM $MgCl_2$ and 2.5 U LA Taq DNA polymerase (TAKARA, Otsu, Shiga, Japan), using a T-GRADIENT Thermocycler (Biometra GmbH, Göttingen, Germany) or a GeneAmp PCR system 9700 (Perkin-Elmer Applied Biosystems, Foster City, CA, USA). The amplification procedure consisted of initial denaturation at 96 °C for 5 min, 35 cycles of denaturation at 96 °C for 30 s, annealing at 60 °C for 30 s and extension at 72 °C for 2 or 3 min for each fragment, followed by the last extension at 72 °C for 7 or 10 min.

Each of the first PCR products was divided into several segments encompassing each exon, and was amplified using primers described in Table 3 (second PCR). Each second PCR and PCR for exon 7 were performed in 25 μl reaction mixtures containing 1 μl amplified PCR products, 0.4 pM each primer, 0.2 mM dNTPs, 2 mM $MgCl_2$ and 1 U of AmpliTaq Gold DNA polymerase (Perkin-Elmer Applied Biosystems), using a T-GRADIENT Thermocycler or a GeneAmp PCR system 9700. The amplification condition consisted of initial denaturation at 96 °C for 10 min, 35 cycles of denaturation at 96 °C for 30 s, annealing at 64–66 °C for 30 s and extension at 72 °C for 30 s, followed by the last extension at 72 °C for 4 min. Fluorescence-based automated cycle sequencing of PCR products was performed using ABI 3100 sequencer (ABI PRISM; Applied Biosystems, Foster City, CA, USA) with the dye-terminator method, according to the manufacturer's instructions (BigDye ver3.1 Cycle Sequencing-Ready Reaction Kit).

Genotyping of *LILRA2* rs3760856, rs28384501, rs28384502 was performed similarly, using nested PCR followed by direct sequencing. For the genotyping of rs2241524, a specific primer set LILRA2-SF and -SR was designed for a single-step PCR-direct sequencing.

Polymorphism screening, haplotype determination and genotyping of LILRA1

Polymorphisms of *LILRA1* gene were screened using nested PCR followed by direct sequencing as in *LILRA2*. Genomic DNA samples from 16 healthy individuals were used for screening. The *LILRA1* exon–intron structure was elucidated by comparing the *LILRA1* mRNA sequence (NM_006863) with chromosome 19 contig sequences in the GenBank (AC009892) as well as in the Celera Discovery System (http://www.celera.com). Whereas *LILRA1* exon 10 comprised 377 bp containing 258 bp 3′-untranslated region (UTR) according to GenBank NM_006863 sequence, it has elongated 3′-UTR sequence (1623 bp) in the Celera database. Therefore, we set the primers to cover whole *LILRA1* mRNA sequence suggested by the Celera Discovery System. Primer set for nested first PCR was placed within the promoter region and within the intron 7 (LILRA1-sF1/LILRA1-sR1) (Table 4), and the other primer set was placed within the intron 7 and at 3′-flanking region (LILRA1-sF2/LILRA1-sR2) (Table 4). Each of the first PCR products was divided into several segments for second PCR-direct sequencing (Table 4).

LILRA1 haplotypes were determined from the segregation pattern of the 31 Japanese families. In the

Table 4 Primers for PCR-direct sequencing and PCR-SSCP of *LILRA1*

Fragment	*Name*	*Primer**	*Position*
Nested	LILRA1-sF1	CTGTGTATACGAATGGCAGA	Promoter
	LILRA1-sR1	TCTTAGTGTCCAGAGCTCTC	int7
Nested	LILRA1-sF2	CCTTGTCCAATCACTGGATA	int7
	LILRA1-sR2	TCAAATGTTTGGCCTGGCAC	3′ franking
Promoter	LILRA1-1F	GTGTATACGAATGGCAGACT	Promoter
	LILRA1-1R	ACCACTGAATGGAGGTGGG	Promoter
Promoter	LILRA1-2F	ACTGTCATTGCAGATCCCGA	Promoter
	LILRA1-2R	TGAGCTTTGATTTGGGGAGT	Promoter
Promoter–int1	LILRA1-3F	GTCATGTAGGCAGCGGATG	Promoter
	LILRA1-3R	TTCCCTTTCCTTCTCACAGC	int1
int1–int2	LILRA1-4F	GATGGATGGCTGAAGGAGG	int1
	LILRA1-4R	GTCCCTCCTAGGTTAGAAGC	int2
ex2–ex4	LILRA1-5F	CTGATCTGTCTCAGTGAGAT	ex2–int2
	LILRA1-5R	CTCTATACAGACGGTACTCC	ex4
ex4–ex5	LILRA1-6F	TCTGGTGTCAGGGGATCCT	ex4
	LILRA1-6R	TGTGAGTTCAGGCATTGTGG	ex5
ex5–ex6	LILRA1-7F	GCAGCTTCATTCTGTGTAAG	ex5
	LILRA1-7R	TCTCCCTCCTTATACAGAAC	ex6
ex6–ex7	LILRA1-8F	CCTCCAGTGTGTTTCTGATG	ex6
	LILRA1-8R	TGCACCGAGATGAAGGGTCT	ex7
int6–int7	LILRA1-9F	TCACCCATCCTTCTTCTCTC	int6
	LILRA1-9R	TAGTGTCCAGAGCTCTCCTG	int7
int7–int8	LILRA1-10F	GAACTCCTGACCTCATGATC	int7
	LILRA1-10R	CTTGACAGGACCTGACCCT	int8
int8–ex10	LILRA1-11F	CCTAGAACTCATGTCAGAAG	int8
	LILRA1-11R	ACCTCCTGGCATCATCAGAT	ex10
ex10	LILRA1-12F	GAAGAATGTACCCTTCAGAG	ex10
	LILRA1-12R	CTGCACAGGTAGCATGTGA	ex10
ex10	LILRA1-13F	TCTGAACCCTACGAGCCCT	ex10
	LILRA1-13R	ATGCTAGGACTCAAGTCCTC	ex10
ex10	LILRA1-14F	TCTGAATTGTCGCAAACAGC	ex10
	LILRA1-14R	TTCTAGAGGGTAGATGGCGA	ex10
ex10–3′ flanking	LILRA1-15F	CATTCACCGTCTACCCTCTA	ex10
	LILRA1-15R	CCTGGCACAACCAAACTAGAA	3′-flanking

Abbreviations: ex, exon; int, intron.
*These were designed according to the genomic DNA sequence containing human *LILRA1* (GenBank accession no. AC009892).

case–control studies, *LILRA1* haplotypes were determined using a fragment containing tag SNPs on the assumption that these haplotypes are conserved in Japanese.

The typing of haplotypes *LILRA1.PC01* and *LILRA1.PC02* was performed using the PCR/single-stranded conformation polymorphism (SSCP) method. A 516 bp fragment containing seven polymorphic sites (*IVS1+78G>A*, *IVS1+163A>C*, *c.-44G>T*, *c.-37C>T*, *c.13G>C*, *c.18A>G* and *c.34A>G*) was amplified using a primer set for direct sequencing (LILRA1-4F and LILRA1-4R) (Table 4). The amplified DNA was analyzed using SSCP. One microliter of solution containing the PCR product was mixed with 7 μl of denaturing solution (95% formamide, 20 mM EDTA, 0.05% bromphenol blue, 0.05% xylene cyanol FF). The mixtures were denatured at 96 °C for 5 min and immediately cooled on ice. One microliter of the mixtures was applied to polyacrylamide gel (acrylamide:bisacrylamide = 49:1). Electrophoresis was carried out in 0.5 × TBE (45 mM Tris-borate (pH8.0), 1 mM EDTA) under constant current of 20 mA per gel, 20 °C for 100 min in 10% polyacrylamide gel using a minigel electrophoresis apparatus with a constant temperature control system (90 × 80 × 1 mm, AE-8450, AB-1600 and AE-6370; ATTO, Tokyo, Japan). Single-stranded DNA fragments in the gel were visualized by silver staining (Daiichi Chemicals, Tokyo, Japan).

RT–PCR

Total RNA was extracted from peripheral blood mononuclear cells (PBMCs) using the PAXgene kit (Qiagen). First-strand cDNA was synthesized using Oligo(dT) primer (Promega, Madison, WI, USA) and ReverTra Ace (Toyobo, Osaka, Japan). To detect the difference between transcripts of GG and AA genotypes, RT–PCR was performed using primers designed within exon 6 and 7 (5′-CAGCAGAACCAGGCTGAATT-3′ and 5′-GTGTAATCCTGGGGGTGTTG-3′). One microliter of template cDNA solution was placed into 25 μl of reaction solution, and amplification was performed using AmpliTaq Gold DNA polymerase (Perkin-Elmer). The amplification conditions consisted of initial denaturation at 96 °C for 10 min, 35 cycles of denaturation at 96 °C for 30 s, annealing at 58 °C for 30 s and extension at 72 °C for 30 min, followed by the last extension at 72 °C for 2 min using GeneAmp PCR system 9700 (Perkin-Elmer Applied Biosystems). Detection of splicing isoform was performed using Agilent 2100 Bioanalyzer (Agilent Technologies, Palo Alto, CA, USA).

Flow cytometric analysis

Surface expression intensity of LILRA2 in peripheral blood monocytes was examined in two healthy donors with *LILRA2* rs2241524 G/G and two with A/A genotype by two-color flow cytometry, using rat

anti-ILT1 mAb 135[14] and PE-conjugated goat F(ab')$_2$ fragment anti-rat IgG (H + L) Ab (Beckman Coulter), as well as fluorescein-isothiocyanate-conjugated anti-CD14 mAb (Beckman Coulter).

Statistical analysis

The frequencies of the *LILRA2* genotypes were compared between groups using the χ^2-test or Fischer's exact test. Statistical analyses were performed using StatView version 5.0 for Windows (Abacus Concepts Inc., Berkeley, CA, USA). LD analysis and estimation of haplotype frequencies were performed by the Estimation-Maximization algorithm using SNPAlyze program (DYNACOM, Mobara, Japan).

Acknowledgements

We are indebted to Dr Jun Ohashi (The University of Tokyo) and Dr Ryosuke Kimura (Tokai University) for their helpful suggestions. Sequence accession number: The nucleotide sequence data reported in this paper have been submitted to the DDBJ database and have been assigned the accession numbers AB375279-AB375302. This work was supported by Grant-in-Aid for Scientific Research on Priority Areas 'Applied Genomics' from the Ministry of Education, Culture, Sports, Science and Technology of Japan, Grant-in-Aid for Scientific Research (B) from Japan Society for the Promotion of Science (JSPS), grants from the Ministry of Health, Labour and Welfare of Japan, Takeda Science Foundation and Japan Rheumatism Foundation.

Conflict of interest

There is no conflict of interest to disclose.

References

1 Borges L, Hsu ML, Fanger N, Kubin M, Cosman D. A family of human lymphoid and myeloid Ig-like receptors, some of which bind to MHC class I molecules. *J Immunol* 1997; **159**: 5192–5196.

2 Colonna M, Navarro F, Bellon T, Llano M, Garcia P, Samaridis J *et al*. A common inhibitory receptor for major histocompatibility complex class I molecules on human lymphoid and myelomonocytic cells. *J Exp Med* 1997; **186**: 1809–1818.

3 Cosman D, Fanger N, Borges L, Kubin M, Chin W, Peterson L *et al*. A novel immunoglobulin superfamily receptor for cellular and viral MHC class I molecules. *Immunity* 1997; **7**: 273–282.

4 Wende H, Colonna M, Ziegler A, Volz A. Organization of the leukocyte receptor cluster (LRC) on human chromosome 19q13.4. *Mamm Genome* 1999; **10**: 154–160.

5 Wende H, Volz A, Ziegler A. Extensive gene duplications and a large inversion characterize the human leukocyte receptor cluster. *Immunogenetics* 2000; **51**: 703–713.

6 Wilson MJ, Torkar M, Haude A, Milne S, Jones T, Sheer D *et al*. Plasticity in the organization and sequences of human KIR/ILT gene families. *Proc Natl Acad Sci USA* 2000; **97**: 4778–4783.

7 Lindqvist AK, Steinsson K, Johanneson B, Kristjansdottir H, Arnasson A, Grondal G *et al*. A susceptibility locus for human systemic lupus erythematosus (hSLE1) on chromosome 2q. *J Autoimmun* 2000; **14**: 169–178.

8 Moser KL, Neas BR, Salmon JE, Yu H, Gray-McGuire C, Asundi N *et al*. Genome scan of human systemic lupus erythematosus: evidence for linkage on chromosome 1q in African-American pedigrees. *Proc Natl Acad Sci USA* 1998; **95**: 14869–14874.

9 Kubagawa H, Burrows PD, Cooper MD. A novel pair of immunoglobulin-like receptors expressed by B cells and myeloid cells. *Proc Natl Acad Sci USA* 1997; **94**: 5261–5266.

10 Yamashita Y, Ono M, Takai T. Inhibitory and stimulatory functions of paired Ig-like receptor (PIR) family in RBL-2H3 cells. *J Immunol* 1998; **161**: 4042–4047.

11 Ujike A, Takeda K, Nakamura A, Ebihara S, Akiyama K, Takai T. Impaired dendritic cell maturation and increased T_H2 responses in PIR-B $^{-/-}$ mice. *Nat Immunol* 2002; **3**: 542–548.

12 Nakamura A, Kobayashi E, Takai T. Exacerbated graft-versus-host disease in *Pirb*$^{-/-}$ mice. *Nat Immunol* 2004; **5**: 623–629.

13 Cella M, Jarrossay D, Facchetti F, Alebardi O, Nakajima H, Lanzavecchia A *et al*. Plasmacytoid monocytes migrate to inflamed lymph nodes and produce large amounts of type I interferon. *Nat Med* 1999; **5**: 919–923.

14 Nakajima H, Samaridis J, Angman L, Colonna M. Human myeloid cells express an activating ILT receptor (ILT1) that associates with Fc receptor γ-chain. *J Immunol* 1999; **162**: 5–8.

15 Bleharski JR, Li H, Meinken C, Graeber TG, Ochoa MT, Yamamura M *et al*. Use of genetic profiling in leprosy to discriminate clinical forms of the disease. *Science* 2003; **301**: 1527–1530.

16 Tedla N, Gibson K, McNeil HP, Cosman D, Borges L, Arm JP. The co-expression of activating and inhibitory leukocyte immunoglobulin-like receptors in rheumatoid synovium. *Am J Pathol* 2002; **160**: 425–431.

17 Colonna M, Samaridis J, Cella M, Angman L, Allen RL, O'Callaghan CA *et al*. Human myelomonocytic cells express an inhibitory receptor for classical and nonclassical MHC class I molecules. *J Immunol* 1998; **160**: 3096–3100.

18 Shiroishi M, Tsumoto K, Amano K, Shirakihara Y, Colonna M, Braud VM *et al*. Human inhibitory receptors Ig-like transcript 2 (ILT2) and ILT4 compete with CD8 for MHC class I binding and bind preferentially to HLA-G. *Proc Natl Acad Sci USA* 2003; **100**: 8856–8861.

19 Tedla N, Bandeira-Melo C, Tassinari P, Sloane DE, Samplaski M, Cosman D *et al*. Activation of human eosinophils through leukocyte immunoglobulin-like receptor 7. *Proc Natl Acad Sci USA* 2003; **100**: 1174–1179.

20 Sloane DE, Tedla N, Awoniyi M, Macglashan Jr DW, Borges L, Austen KF *et al*. Leukocyte immunoglobulin-like receptors: novel innate receptors for human basophil activation and inhibition. *Blood* 2004; **104**: 2832–2839.

21 Huynh OA, Hampartzoumian T, Arm JP, Hunt J, Borges L, Ahern M *et al*. Down-regulation of leucocyte immunoglobulin-like receptor expression in the synovium of rheumatoid arthritis patients after treatment with disease-modifying anti-rheumatic drugs. *Rheumatology* 2007; **46**: 742–751.

22 Koga T, Inui M, Inoue K, Kim S, Suematsu A, Kobayashi E *et al*. Costimulatory signals mediated by the ITAM motif cooperate with RANKL for bone homeostasis. *Nature* 2004; **428**: 758–763.

23 Tsuchiya N, Kyogoku C, Miyashita R, Kuroki K. Diversity of human immune system multigene families and its implication in the genetic background of rheumatic diseases. *Curr Med Chem* 2007; **14**: 431–439.

24 Tsuchiya N, Honda Z, Tokunaga K. Role of B cell inhibitory receptor polymorphisms in systemic lupus erythematosus: a negative times a negative makes a positive. *J Hum Genet* 2006; **51**: 741–750.

25 Miyashita R, Tsuchiya N, Yabe T, Kobayashi S, Hashimoto H, Ozaki S *et al*. Association of killer cell immunoglobulin-like receptor genotypes with microscopic polyangiitis. *Arthritis Rheum* 2006; **54**: 992–997.

26 Kuroki K, Tsuchiya N, Shiroishi M, Rasubala L, Yamashita Y, Matsuta K *et al*. Extensive polymorphisms of *LILRB1* (*ILT2*, *LIR1*) and their association with HLA-DRB1 shared

epitope negative rheumatoid arthritis. *Hum Mol Genet* 2005; **14**: 2469–2480.

27 Hirayasu K, Ohashi J, Kashiwase K, Takanashi M, Satake M, Tokunaga K *et al*. Long-term persistence of both functional and non-functional alleles at the leukocyte immunoglobulin-like receptor A3 (LILRA3) locus suggests balancing selection. *Hum Genet* 2006; **119**: 436–443.

28 Kyogoku C, Tsuchiya N. A compass that points to lupus: genetic studies on type I interferon pathway. *Genes Immun* 2007; **8**: 445–455.

29 Reumaux D, Duthilleul P, Roos D. Pathogenesis of diseases associated with antineutrophil cytoplasm autoantibodies. *Hum Immunol* 2004; **65**: 1–12.

30 Takahashi S, Fossati L, Iwamoto M, Merino R, Motta R, Kobayakawa T *et al*. Imbalance towards Th1 predominance is associated with acceleration of lupus-like autoimmune syndrome in MRL mice. *J Clin Invest* 1996; **97**: 1597–1604.

31 Ohashi J, Yamamoto S, Tsuchiya N, Hatta Y, Komata T, Matsushita M *et al*. Comparison of statistical power between 2×2 allele frequency and allele positivity tables in case-control studies of complex disease genes. *Ann Hum Genet* 2001; **65**: 197–206.

32 Tsuchiya N, Kobayashi S, Kawasaki A, Kyogoku C, Arimura Y, Yoshida M *et al*. Genetic background of Japanese patients with antineutrophil cytoplasmic antibody-associated vasculitis: association of HLA-DRB1*0901 with microscopic polyangiitis. *J Rheumatol* 2003; **30**: 1534–1540.

33 Tsuchiya N, Kobayashi S, Hashimoto H, Ozaki S, Tokunaga K. Association of *HLA-DRB1*0901-DQB1*0303* haplotype with microscopic polyangiitis in Japanese. *Genes Immun* 2006; **7**: 81–84.

34 Arnett FC, Edworthy SM, Bloch DA, McShane DJ, Fries JF, Cooper NS *et al*. The American Rheumatism Association 1987 revised criteria for the classification of rheumatoid arthritis. *Arthritis Rheum* 1988; **31**: 315–324.

35 Tan EM, Cohen AS, Fries JF, Masi AT, McShane DJ, Rothfield NF *et al*. The 1982 revised criteria for the classification of systemic lupus erythematosus. *Arthritis Rheum* 1982; **25**: 1271–1277.

36 Jennette JC, Falk RJ, Andrassy K, Bacon PA, Churg J, Gross WL *et al*. Nomenclature of systemic vasculitides. Proposal of an international consensus conference. *Arthritis Rheum* 1994; **37**: 187–192.